Electronic Supplementary Information

A Chiral Metal-Organic Framework Fluorescent Sensor incorporating H_8-BINOL

Pattara Siripanich[a], Jierui Zhang[b], Martina Lessio[b], Carol Hua*[a]

[a] *School of Chemistry, The University of Melbourne, Parkville, Victoria 3010, Australia;* [b] *School of Chemistry, University of New South Wales, Kensington, New South Wales 2052, Australia*
Corresponding author e-mail address: carol.hua@unimelb.edu.au

Table of Contents

Experimental

Synthesis of 3,3'-dibromo-5,5',6,6',7,7',8,8'-octahydro-1,1'-binaphthyl-2,2'-diol (Br-H_8-BINOL)

The synthesis was conducted following a literature procedure.[1] (***S***) or (***R***)-5,5',6,6',7,7′,8,8′-Cctahydro-1,1′-binaphthol (**H_8- BINOL**) (1.00 g, 3.40 mmol) was dissolved in CH_2Cl_2 (35 mL) before being cooled in an ice bath to 0 °C. Bromine (0.37 mL, 7.22 mmol) was added dropwise and the reaction stirred for 30 minutes prior to quenching with a saturated solution of Na_2SO_3 (35 mL). The product was extracted with H_2O (2 × 35 mL) and brine (35 mL). The organic layer was dried over anhydrous Na_2SO_4 and the solvent evaporated under reduced pressure. The brown sticky crude oil purified using flash column chromatography with CH_2Cl_2 yielding a yellow-brown solid (74%, 0.905 g). ^{1}H NMR (400MHz, $CDCl_3$) δ (ppm): 7.28 (s, 2H), 5.11 (s, 2H), 2.76-2.73 (m, 4H), 2.33-2.25 (m, 2H), 2.13-2.06 (m, 2H), 1.77-1.61 (m, 8H).

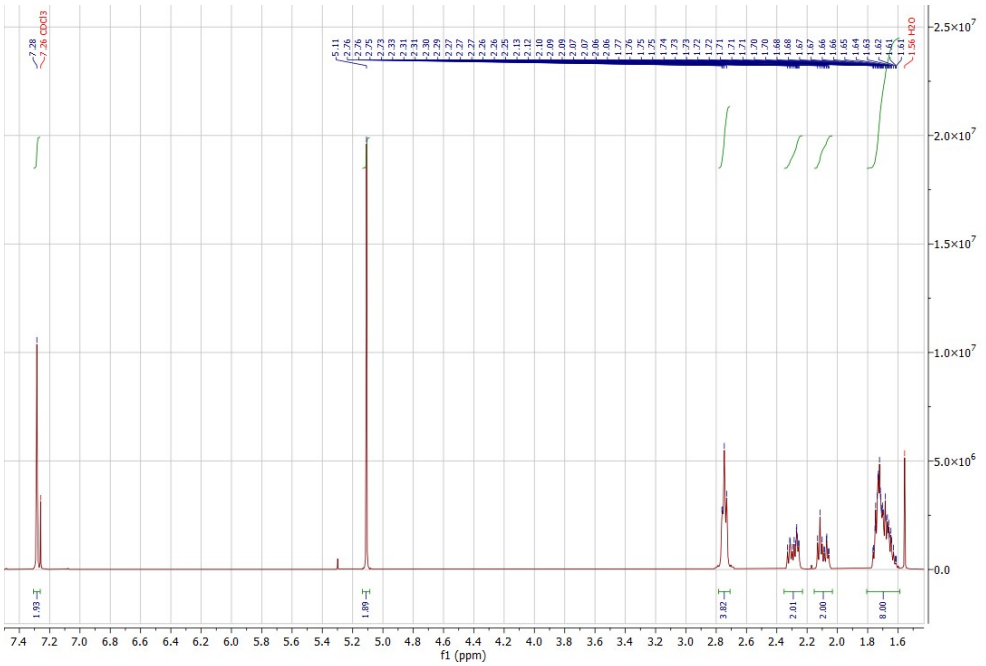

Figure S1. ^{1}H-NMR spectra of **(*S*)-Br-H$_8$-BINOL.**

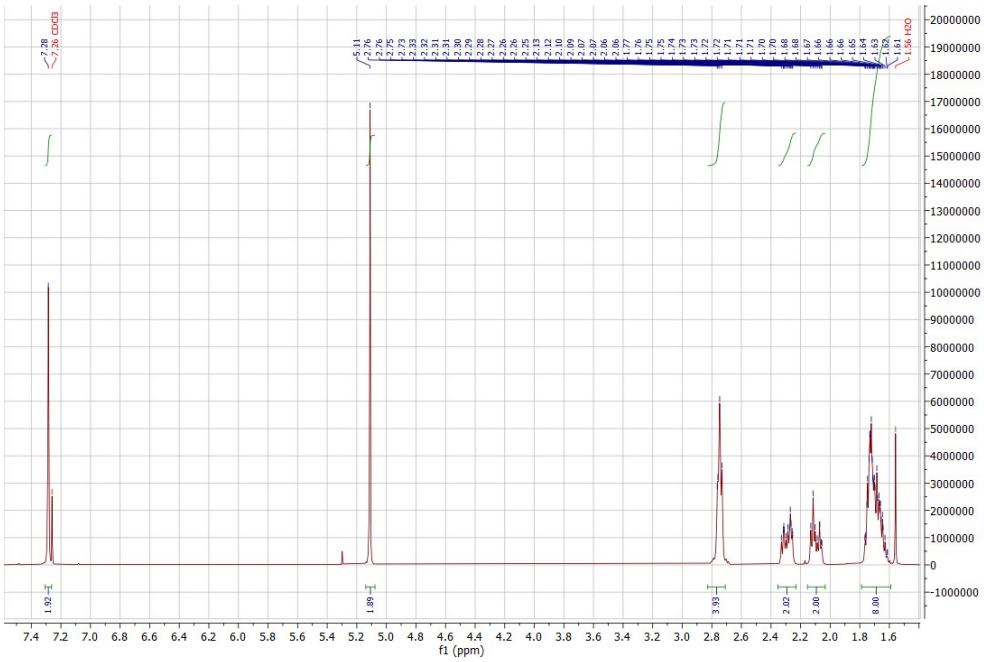

Figure S2. ^{1}H-NMR spectra of **(*R*)-Br-H$_8$-BINOL.**

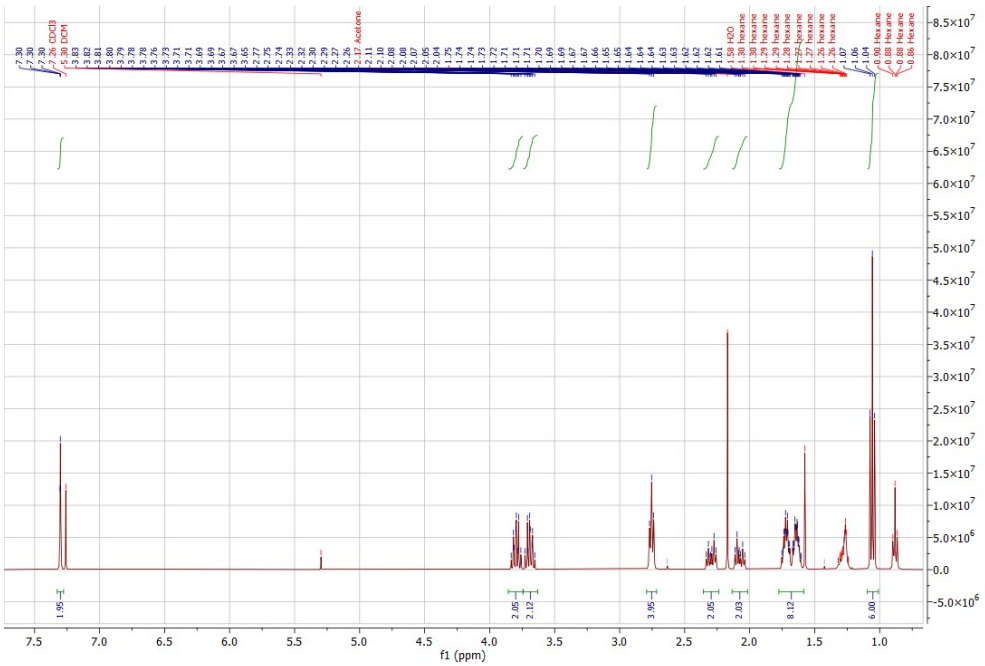

Figure S3. [1]H-NMR spectra of **(*S*)-Br-OEt-H$_8$-BINOL.**

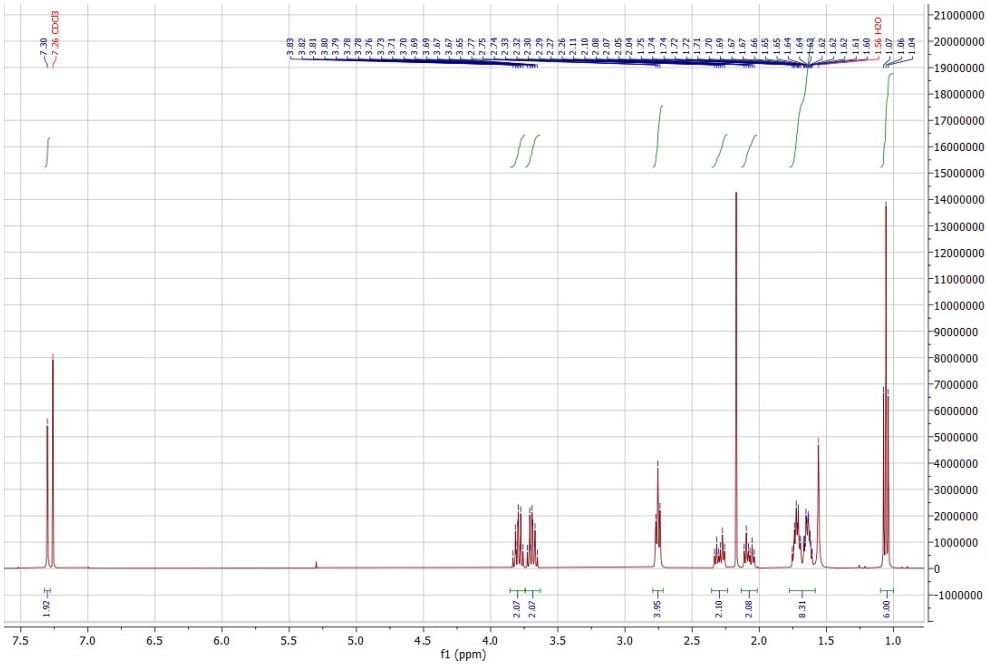

Figure S4. [1]H-NMR spectra of **(*R*)-Br-OEt-H$_8$-BINOL.**

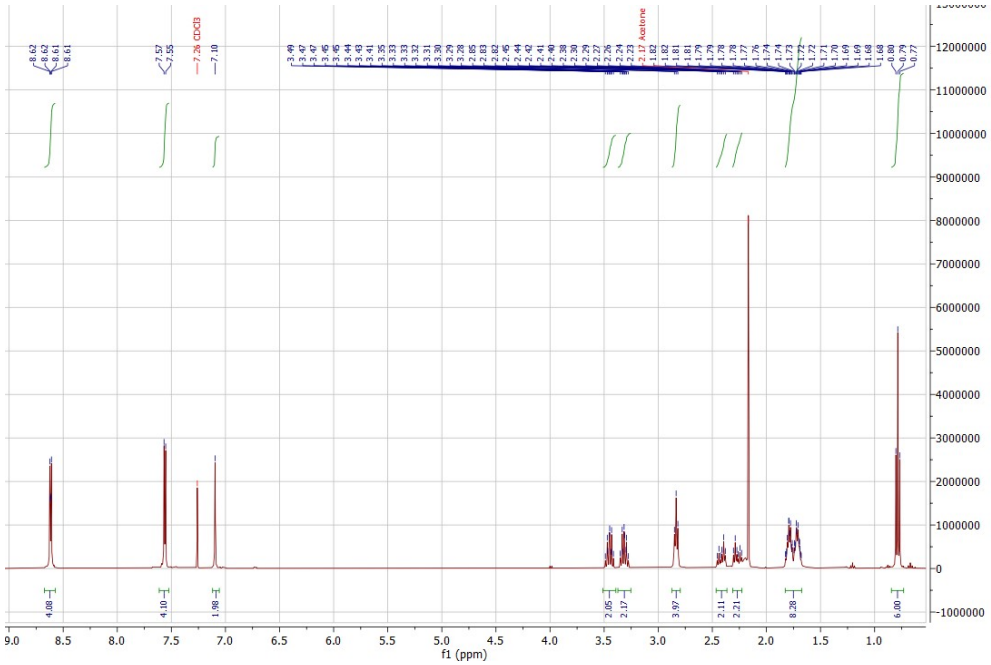

Figure S5. ^{1}H-NMR spectra of **(*S*)-L.**

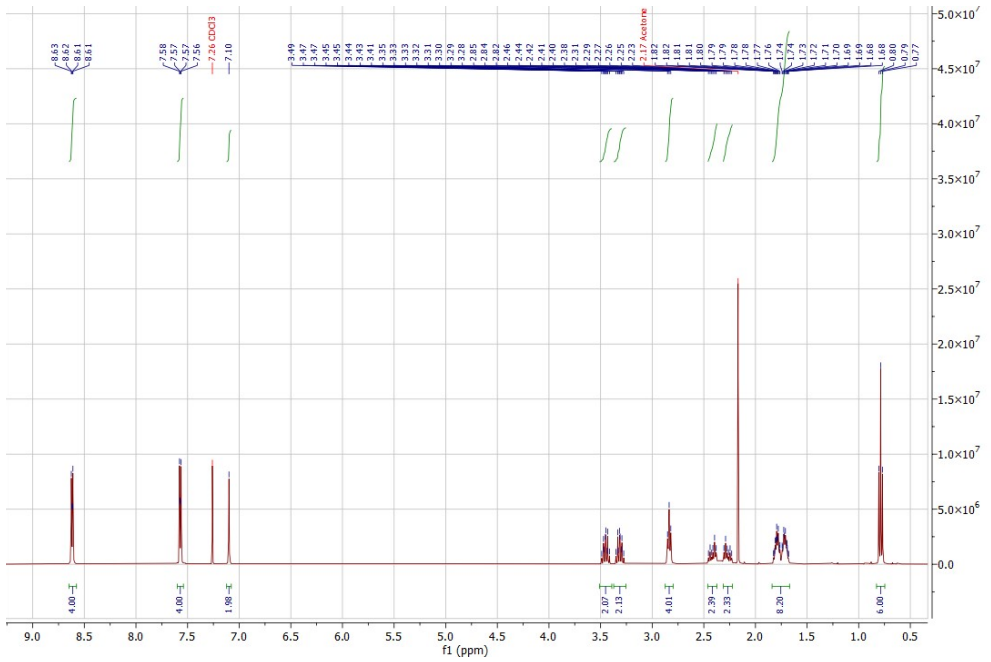

Figure S6. ^{1}H-NMR spectra of **(*R*)-L.**

	(*S*)-1	(*R*)-1
Empirical formula	$C_{121}H_{125}Cd_2N_7O_{17}$	$C_{62}H_{67}CdN_4O_{10}$
Formula weight	2174.07	1140.59
Temperature/K	99.98(10)	100.00(10)
Crystal system	orthorhombic	orthorhombic
Space group	$P2_12_12$	$P2_12_12$
a/Å	20.82810(10)	20.87686(8)
b/Å	18.67620(10)	18.70172(6)
c/Å	15.42900(10)	15.50573(5)
α/°	90	90
β/°	90	90
γ/°	90	90
Volume/Å^3	6001.72(6)	6053.95(3)
Z	2	4
ρ_{calc}g/cm^3	1.203	1.251
μ/mm^{-1}	3.344	3.360
F(000)	2264.0	2380.0
Crystal size/mm^3	0.3 × 0.15 × 0.1	0.3 × 0.2 × 0.2
Radiation	Cu Kα (λ = 1.54184)	Cu Kα (λ = 1.54184)
2θ range for data collection/°	6.356 to 152.986	6.346 to 152.696
Index ranges	$-26 \le h \le 24$, $-23 \le k \le 22$, $-19 \le l \le 18$	$-26 \le h \le 23$, $-22 \le k \le 22$, $-19 \le l \le 19$
Reflections collected	204803	230369
Independent reflections	12291 [R_{int} = 0.0588, R_{sigma} = 0.0180]	12321 [R_{int} = 0.0725, R_{sigma} = 0.0218]
Data/restraints/parameters	12291/59/686	12321/0/689
Goodness-of-fit on F^2	1.088	1.040
Final R indexes [I>=2σ (I)]	R_1 = 0.0435, wR_2 = 0.1324	R_1 = 0.0476, wR_2 = 0.1346
Final R indexes [all data]	R_1 = 0.0442, wR_2 = 0.1332	R_1 = 0.0479, wR_2 = 0.1349
Largest diff. peak/hole / e Å^{-3}	1.39/−0.67	1.55/−1.20
Flack parameter	−0.018(2)	−0.0060(19)

Table S1. Crystallographic parameters for **1**.

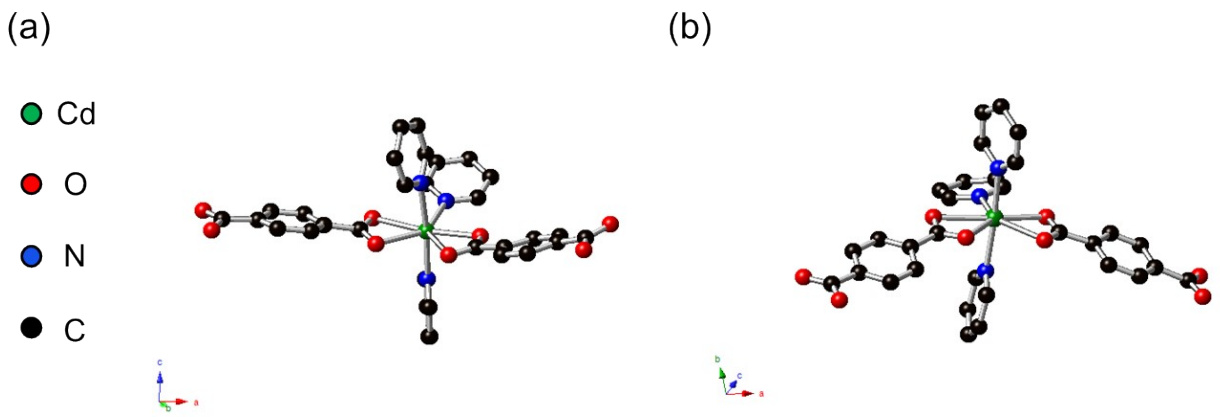

Figure S7. The coordination environments of (a) **(*S*)-1** and (b) **(*R*)-1**.

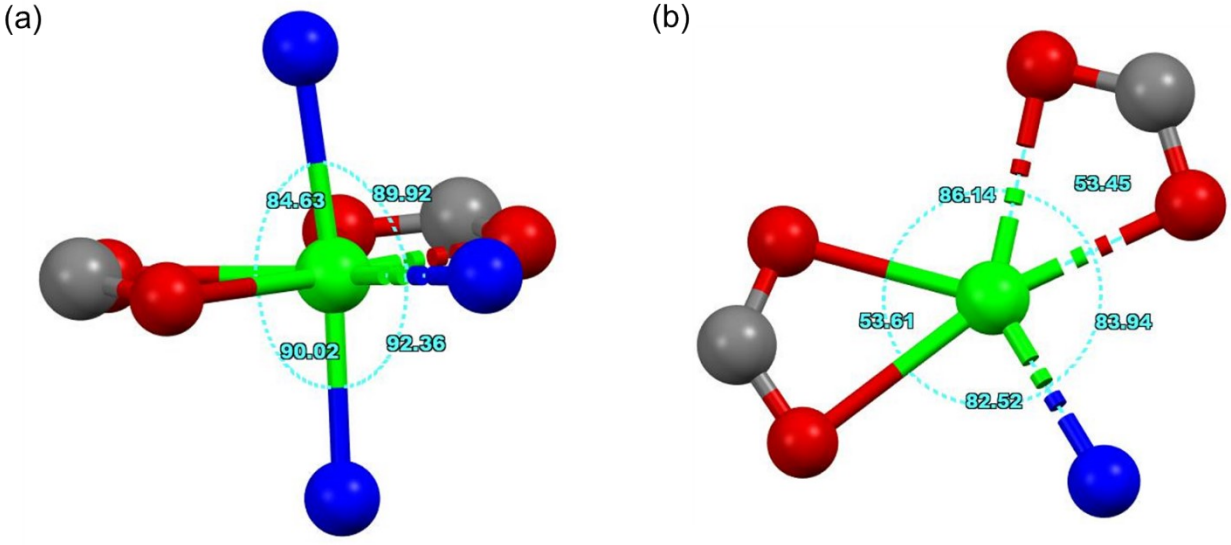

Figure S8. The bond angles in a Cd(II) complex of **(*R*)-1**. (a) axial-equatorial bond angles and (b) equatorial bond angles.

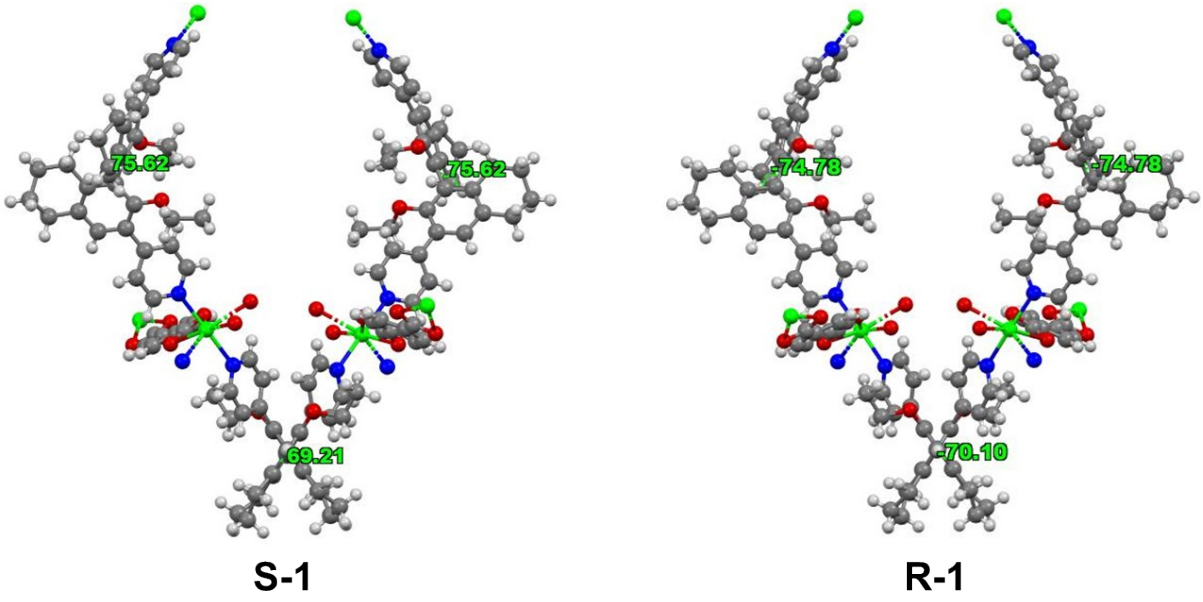

Figure S9. The torsional angle between the naphthyl rings of ***(S)*-1** and ***R*-(1)**

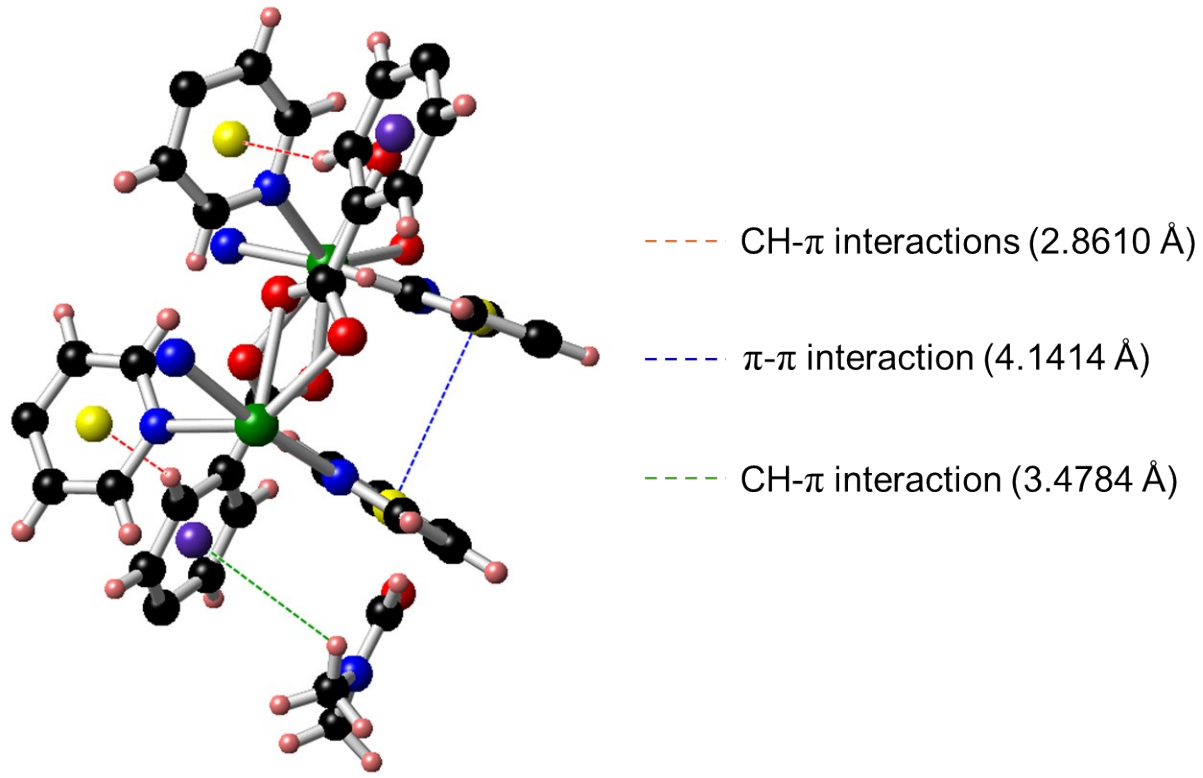

Figure S10. The intermolecular interactions found in (*R*)-**1**.

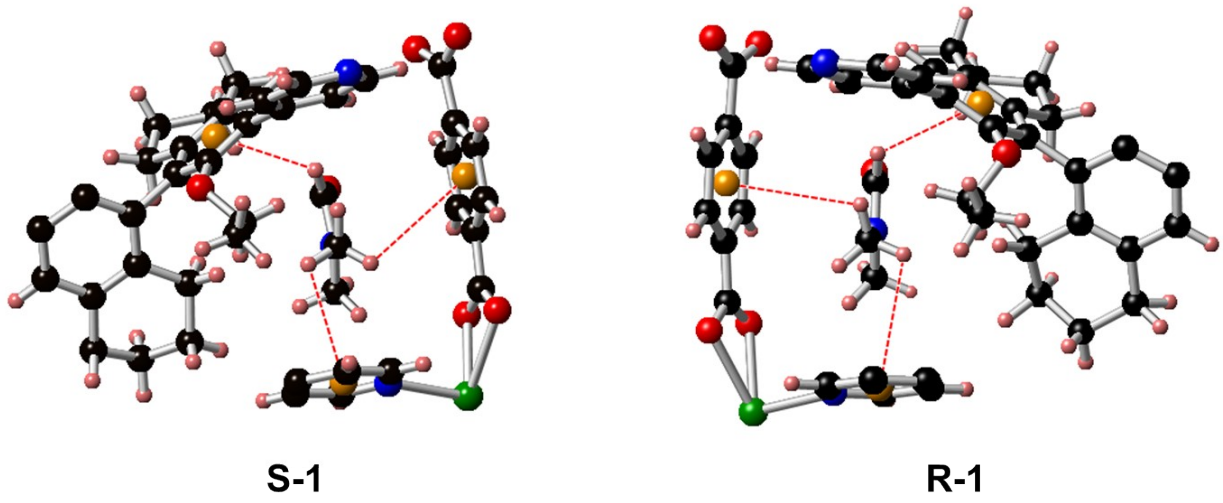

Figure S11. The intermolecular interactions between (*S*)-**1** and (*R*)-**1** and the DMF solvent molecule.

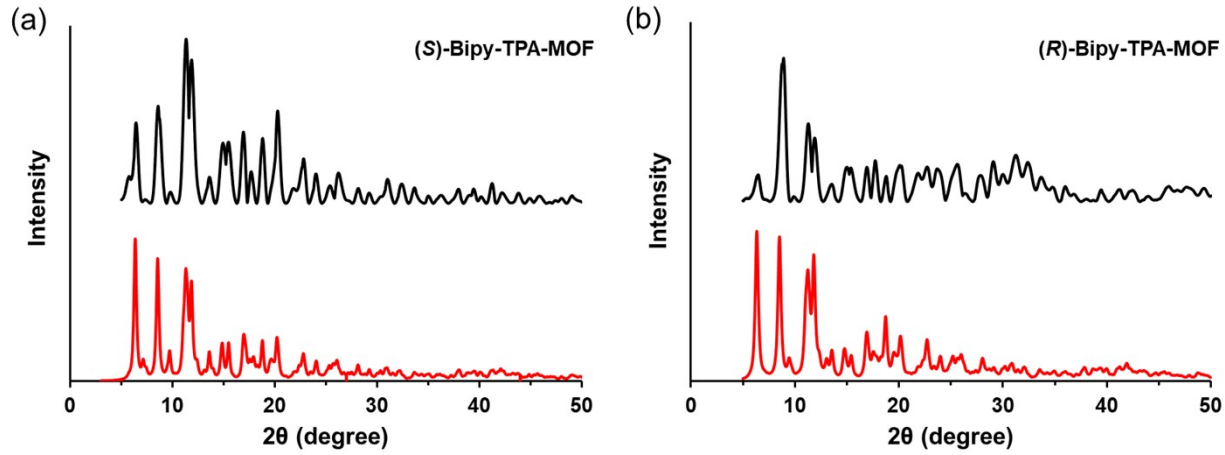

Figure S12. PXRD of (a) **(*S*)-1** and (b) **(*R*)-1** with calculated (red) and experimental (black) patterns.

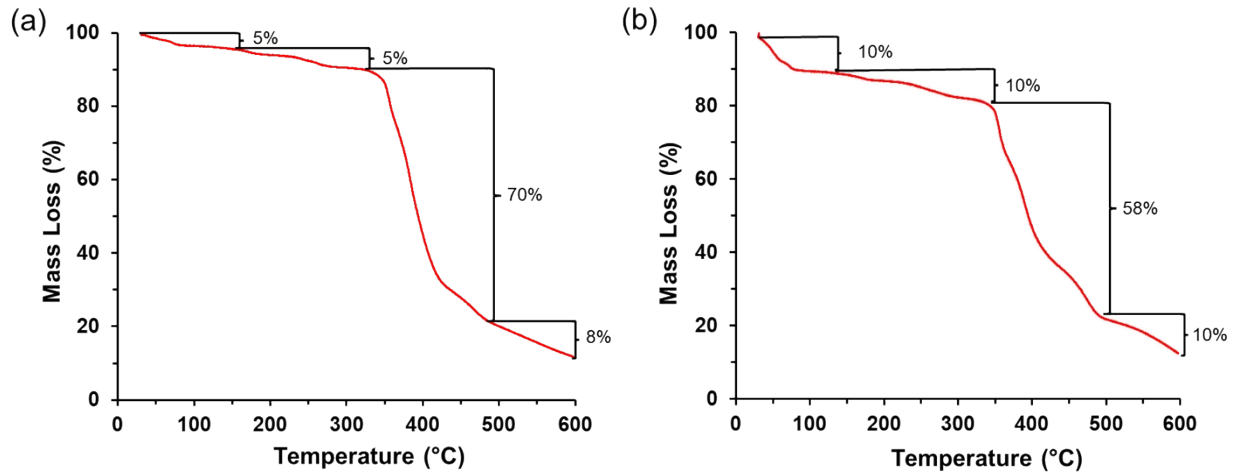

Figure S13. Thermal Gravimetric Analysis (TGA) of (a) **(*S*)-1** and (b) **(*R*)-1**.

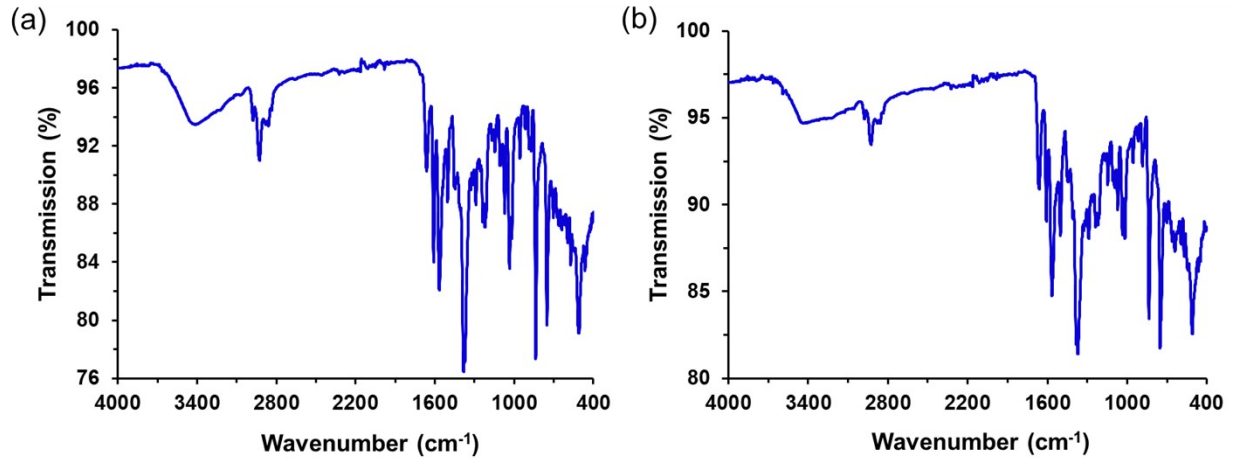

Figure S14. ATR-FTIR spectra of (a) **(*S*)-1** and (b) **(*R*)-1**.

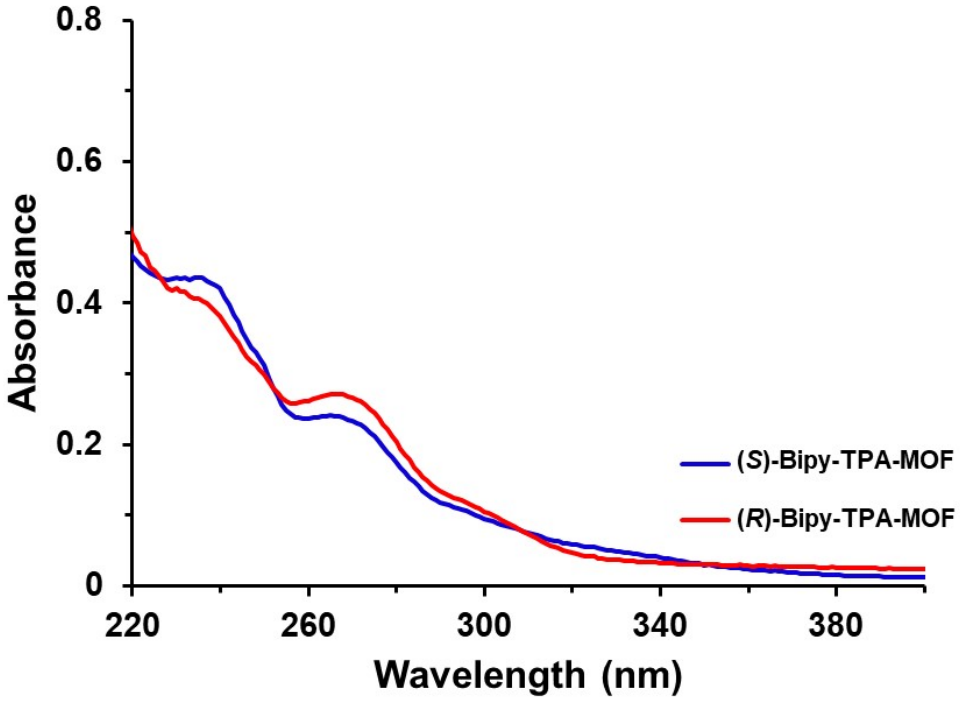

Figure S15. Absorption spectra of **(*S*)-1** (blue) and **(*R*)-1** (red) in ethanol (0.2 g·L^{-1}).

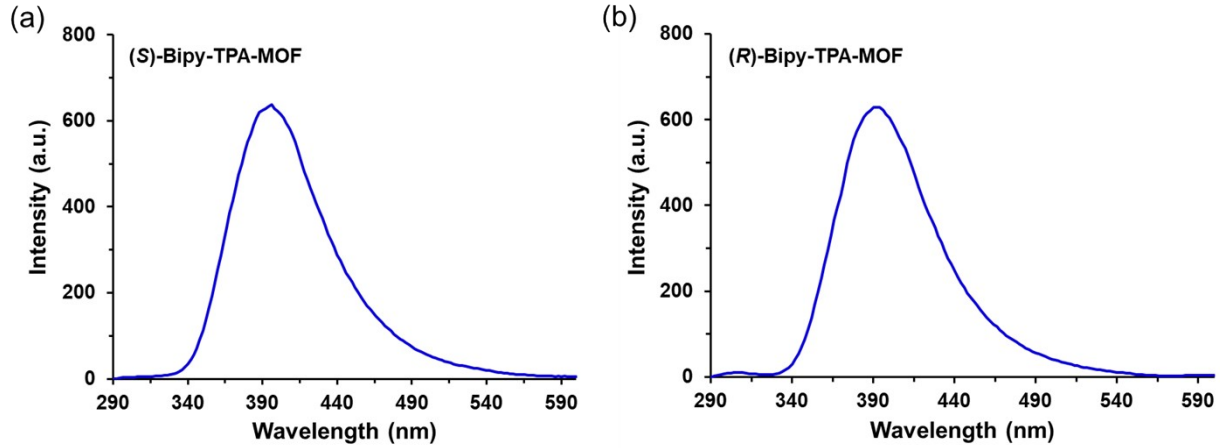

Figure S16. Emission spectra of (a) **(*S*)-1** and (b) **(*R*)-1** in ethanol (λ_{ex} = 270 nm).

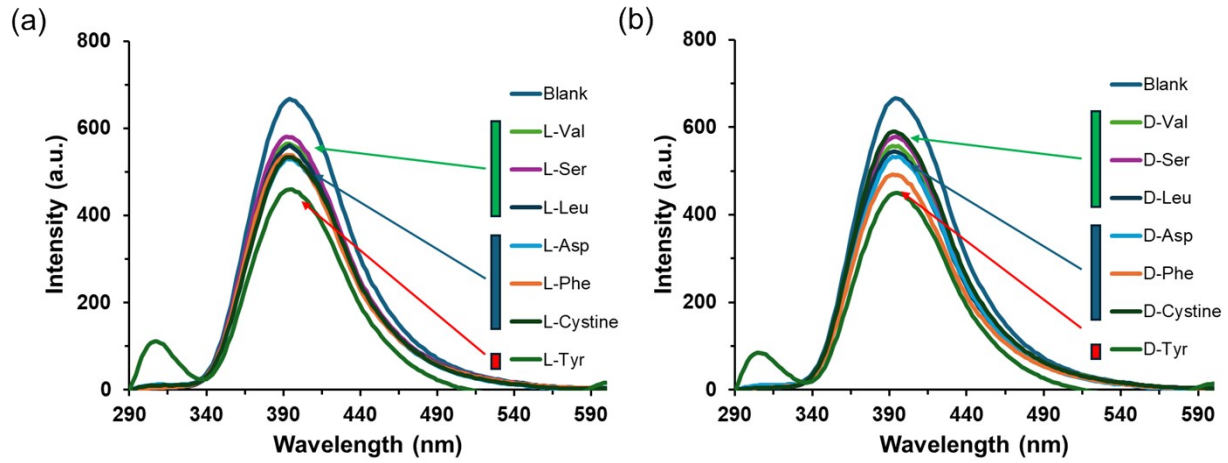

Figure S17. The fluorescence spectra of **(*S*)-1** (0.2 $g \cdot L^{-1}$) with various (a) (*L*)-amino acids, (b) (*D*)-amino acids (520 μM) with an excitation wavelength (λ_{ex}) of 270 nm in ethanol. The color bars indicate quenching affinity of the amino acids' series (Green: slight quenching, Blue: moderated quenching, Red: strong quenching).

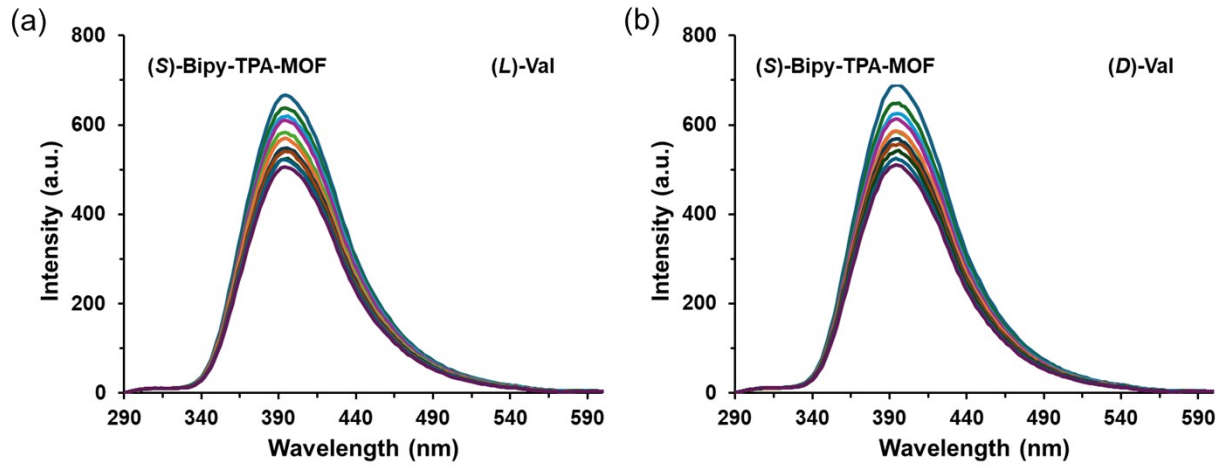

Figure S18. Fluorescence titration spectra of **(*S*)-1** with (a) **(*L*)-Val** and (b) **(*D*)-Val,** ranging from 0 μM to 667 μM of analyte.

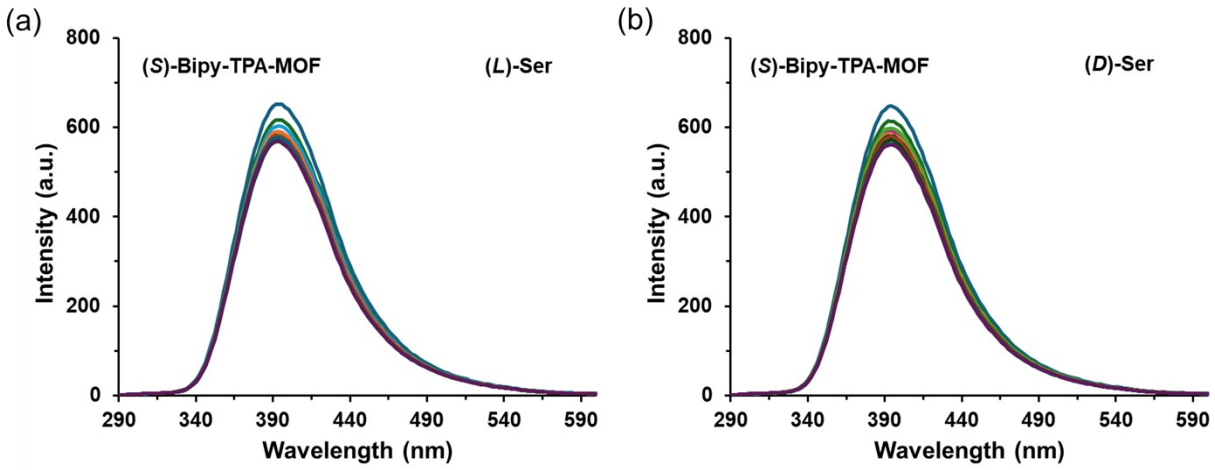

Figure S19. Fluorescence titration spectra of **(*S*)-1** with (a) **(*L*)-Ser** and (b) **(*D*)-Ser,** ranging from 0 μM to 667 μM of analyte.

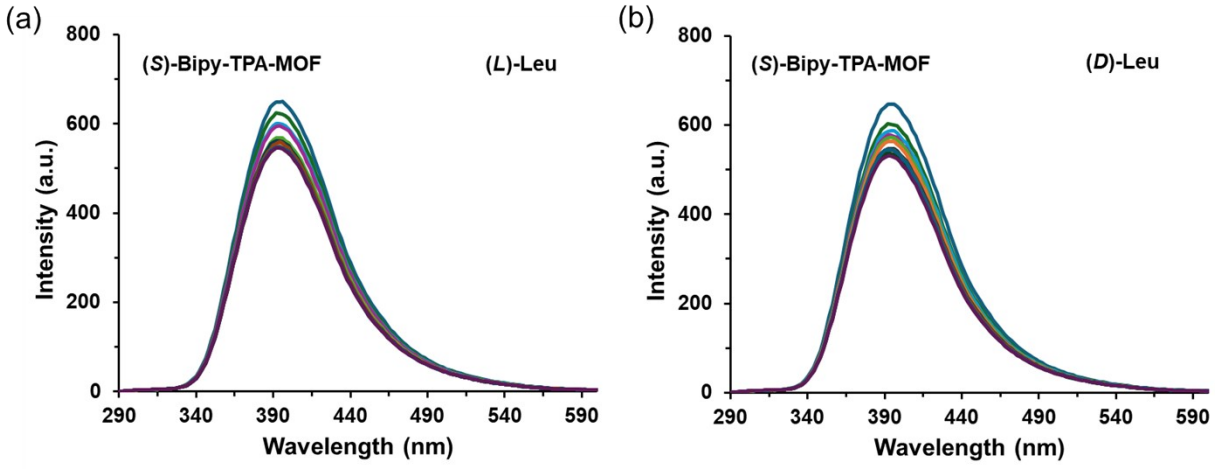

Figure S20. Fluorescence titration spectra of **(*S*)-1** with (a) **(*L*)-Leu** and (b) **(*D*)-Leu,** ranging from 0 μM to 667 μM of analyte.

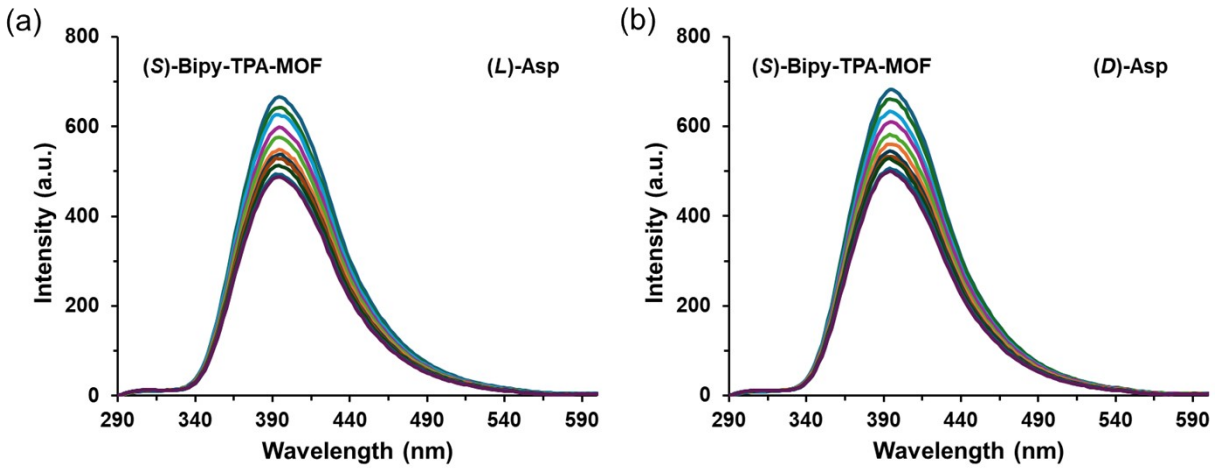

Figure S21. Fluorescence titration spectra of **(*S*)-1** with (a) **(*L*)-Asp** and (b) **(*D*)-Asp,** ranging from 0 μM to 667 μM of analyte.

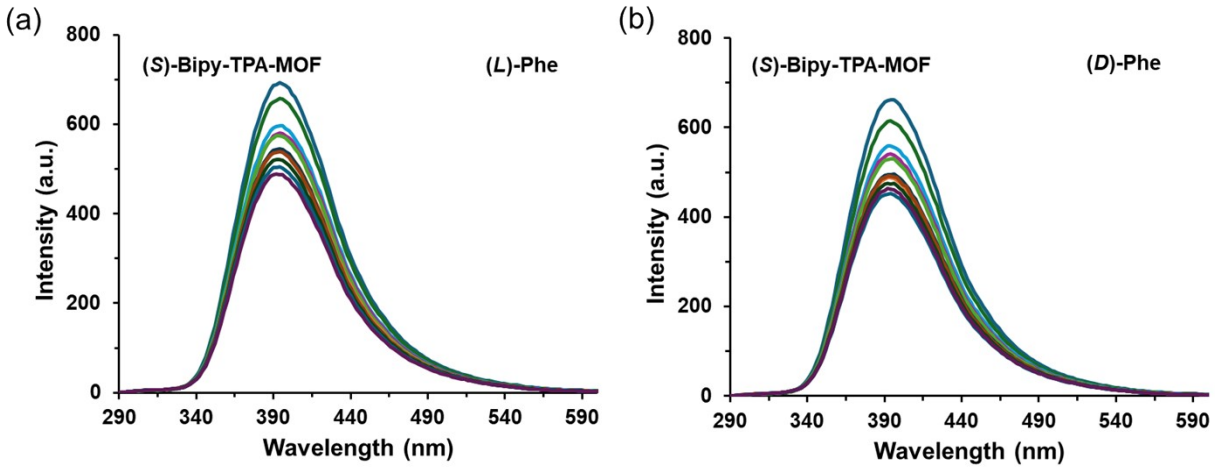

Figure S22. Fluorescence titration spectra of **(*S*)-1** with (a) **(*L*)-Phe** and (b) **(*D*)-Phe,** ranging from 0 μM to 667 μM of analyte.

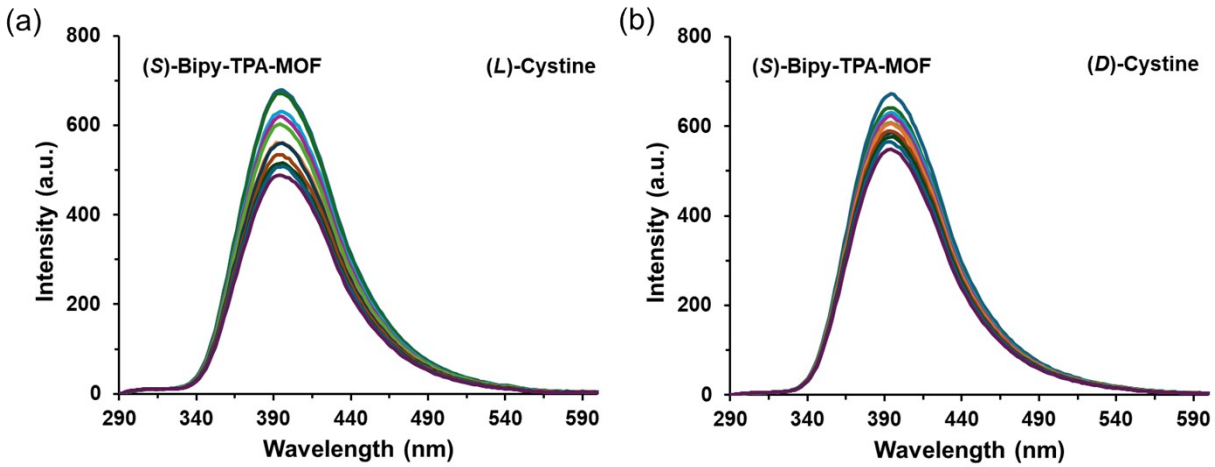

Figure S23. Fluorescence titration spectra of **(*S*)-1** with (a) **(*L*)-Cystine** and (b) **(*D*)-Cystine,** ranging from 0 μM to 667 μM of analyte.

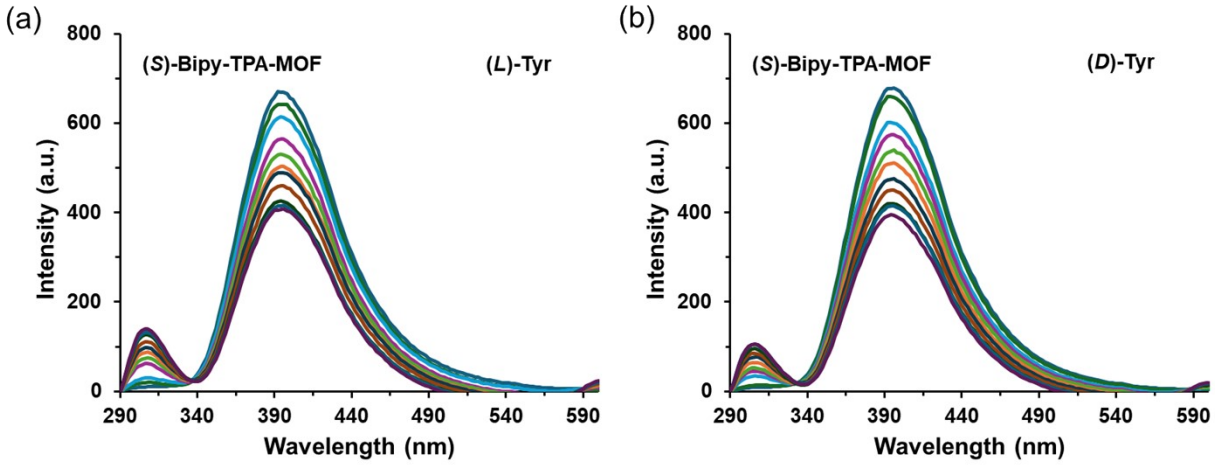

Figure S24. Fluorescence titration spectra of **(*S*)-1** with (a) **(*L*)-Cystine** and (b) **(*D*)-Cystine,** ranging from 0 μM to 667 μM of analyte.

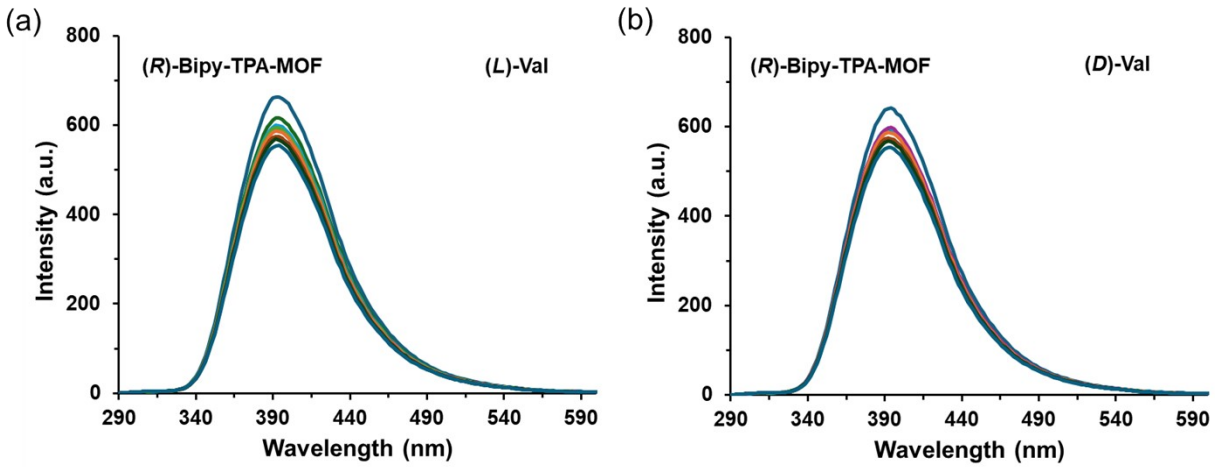

Figure S25. Fluorescence titration spectra of **(*R*)-1** with (a) **(*L*)-Val** and (b) **(*D*)-Val,** ranging from 0 μM to 620 μM of analyte.

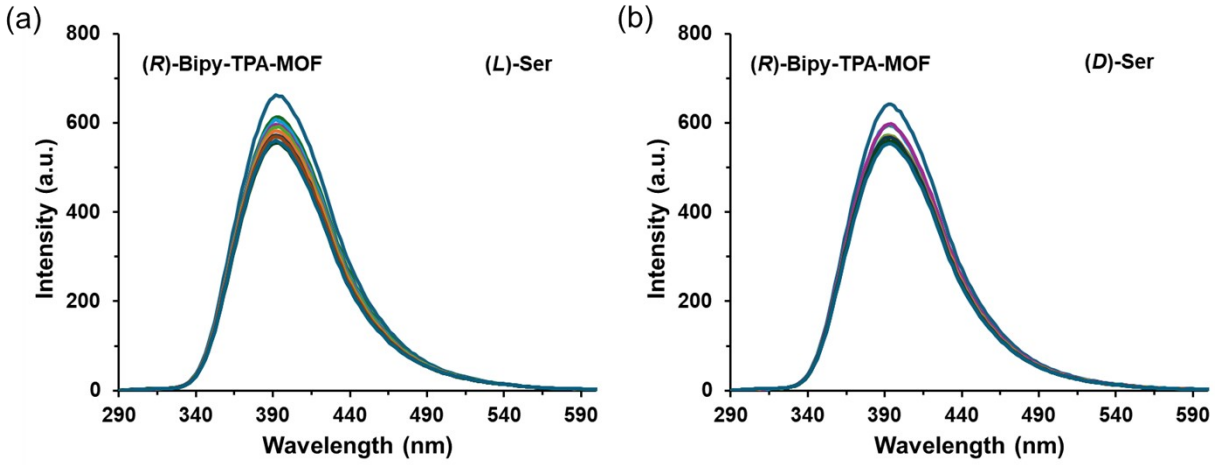

Figure S26. Fluorescence titration spectra of **(*R*)-1** with (a) **(*L*)-Ser** and (b) **(*D*)-Ser,** ranging from 0 μM to 620 μM of analyte.

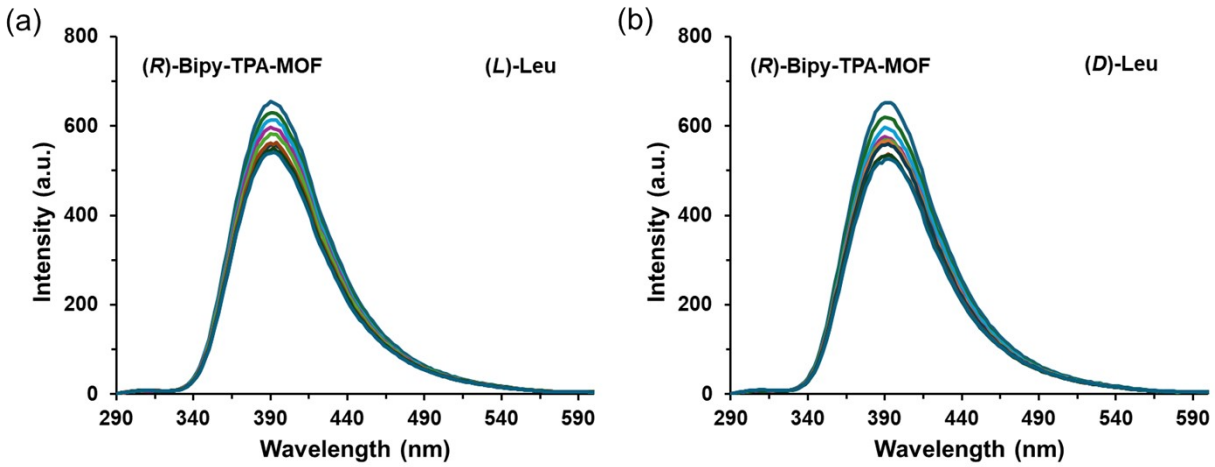

Figure S27. Fluorescence titration spectra of **(*R*)-1** with (a) **(*L*)-Leu** and (b) **(*D*)-Leu,** ranging from 0 μM to 620 μM of analyte.

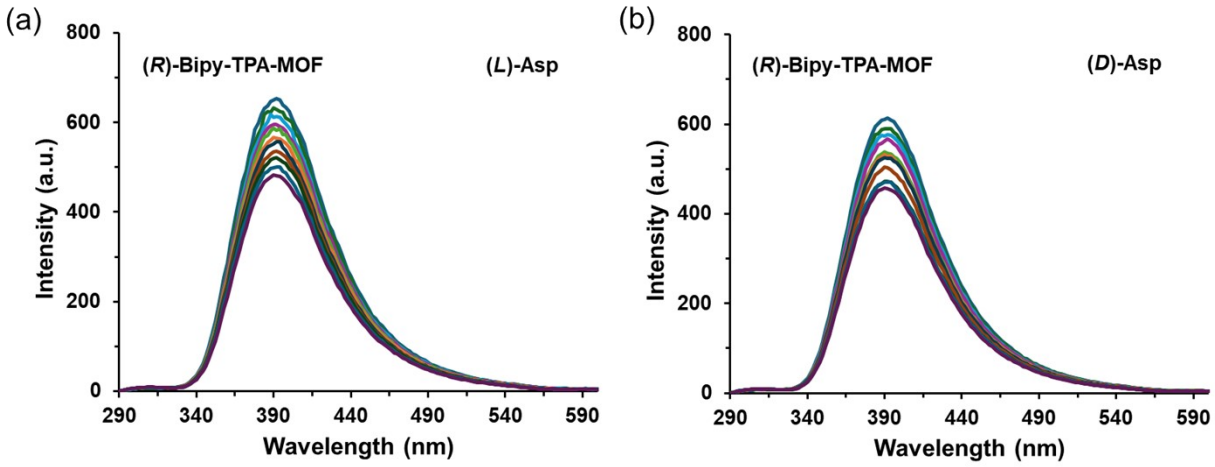

Figure S28. Fluorescence titration spectra of **(*R*)-1** with (a) **(*L*)-Asp** and (b) **(*D*)-Asp,** ranging from 0 μM to 620 μM of analyte.

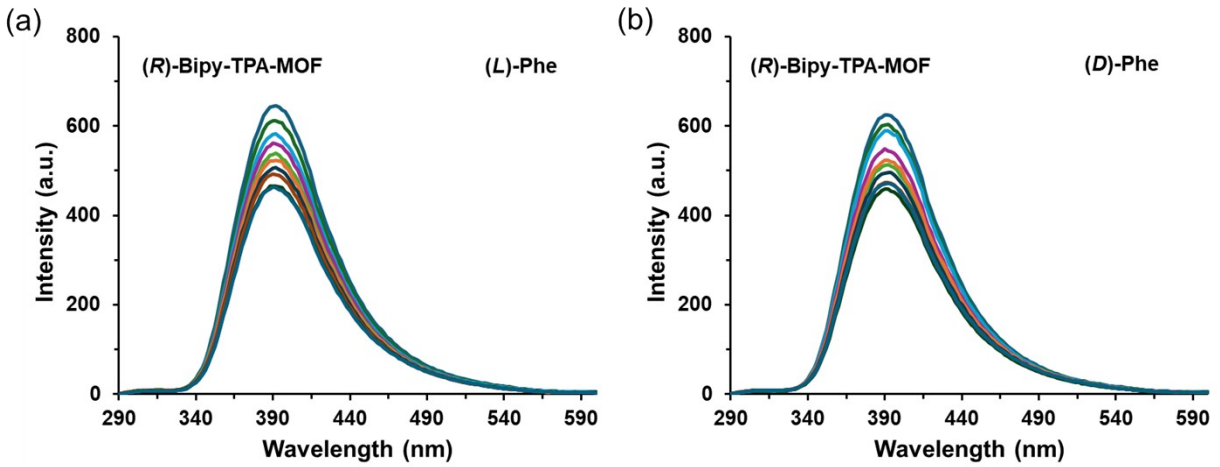

Figure S29. Fluorescence titration spectra of **(*R*)-1** with (a) **(*L*)-Phe** and (b) **(*D*)-Phe,** ranging from 0 μM to 620 μM of analyte.

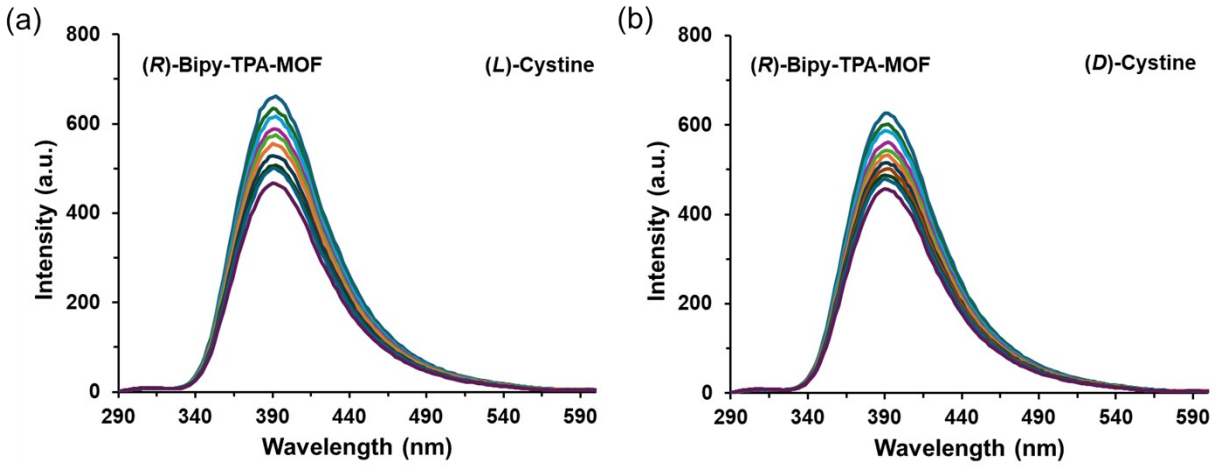

Figure S30. Fluorescence titration spectra of **(*R*)-1** with (a) **(*L*)-Cystine** and (b) **(*D*)-Cystine,** ranging from 0 μM to 620 μM of analyte.

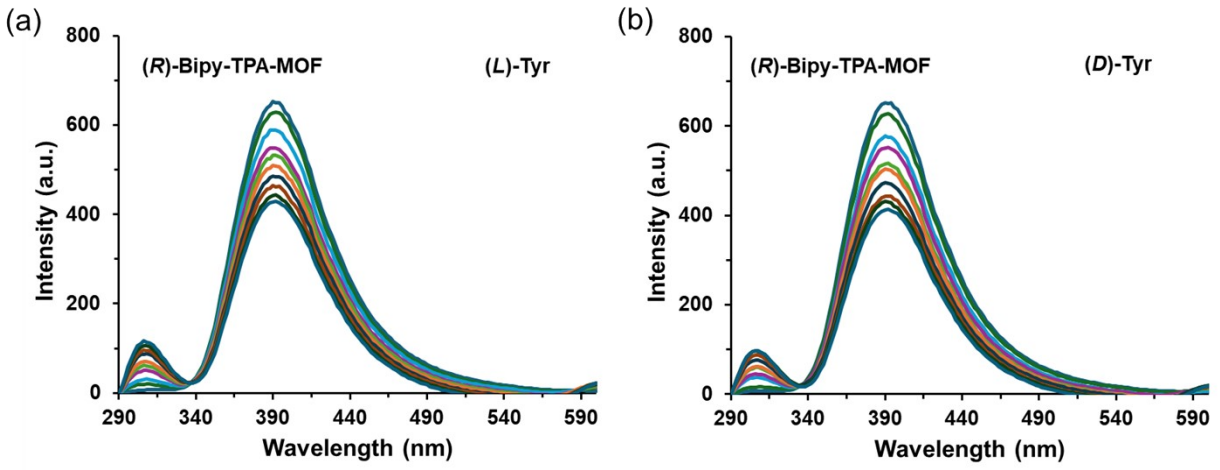

Figure S31. Fluorescence titration spectra of **(*R*)-1** with (a) **(*L*)-Tyr** and (b) **(*D*)-Tyr,** ranging from 0 μM to 620 μM of analyte.

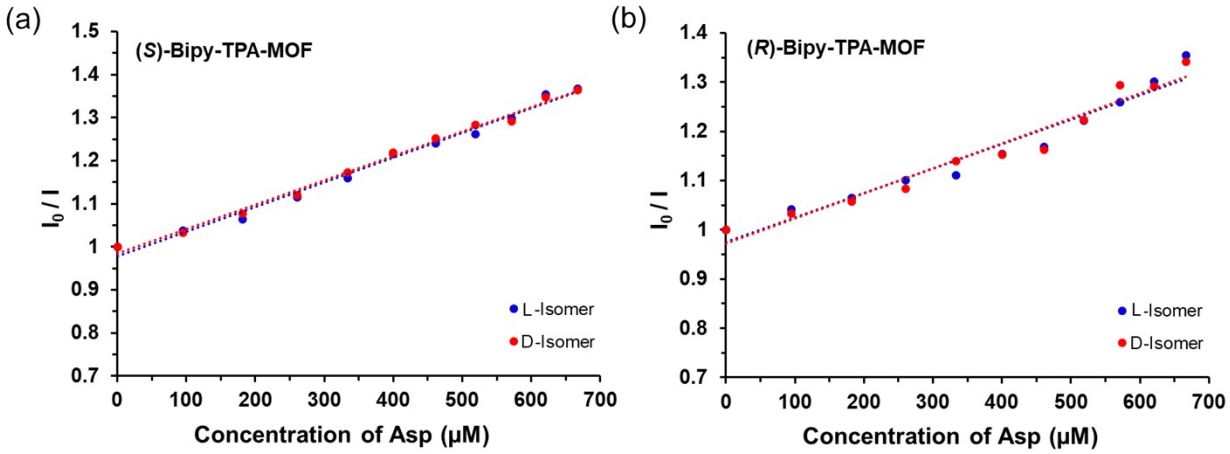

Figure S32. Stern-Volmer plots of (a) **(*S*)-1** and (b) **(*R*)-1** with the enantiomers of aspartic acid (**Asp**).

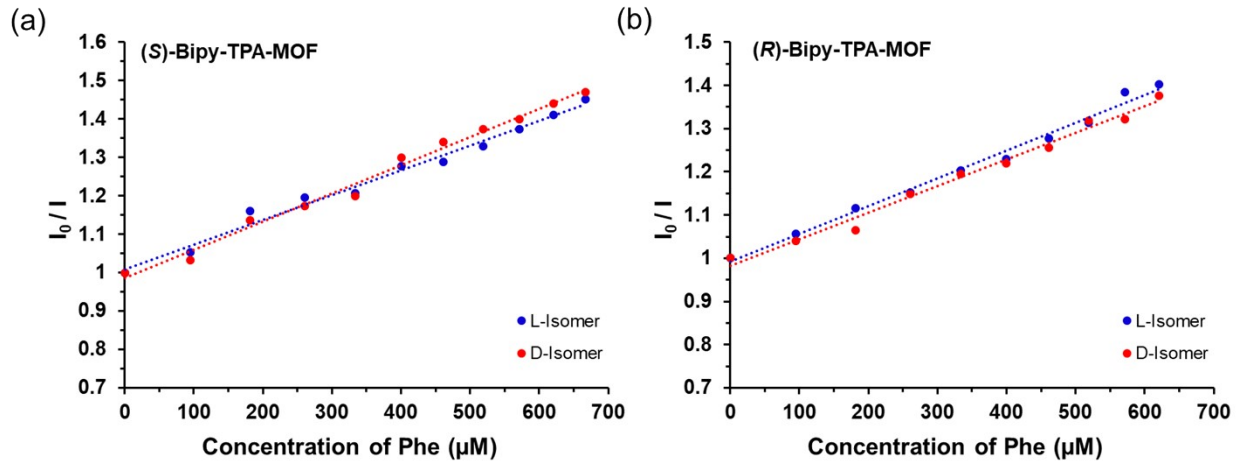

Figure S33. Stern-Volmer plots of (a) **(*S*)-1** and (b) **(*R*)-1** with the enantiomers of phenylalanine (**Phe**).

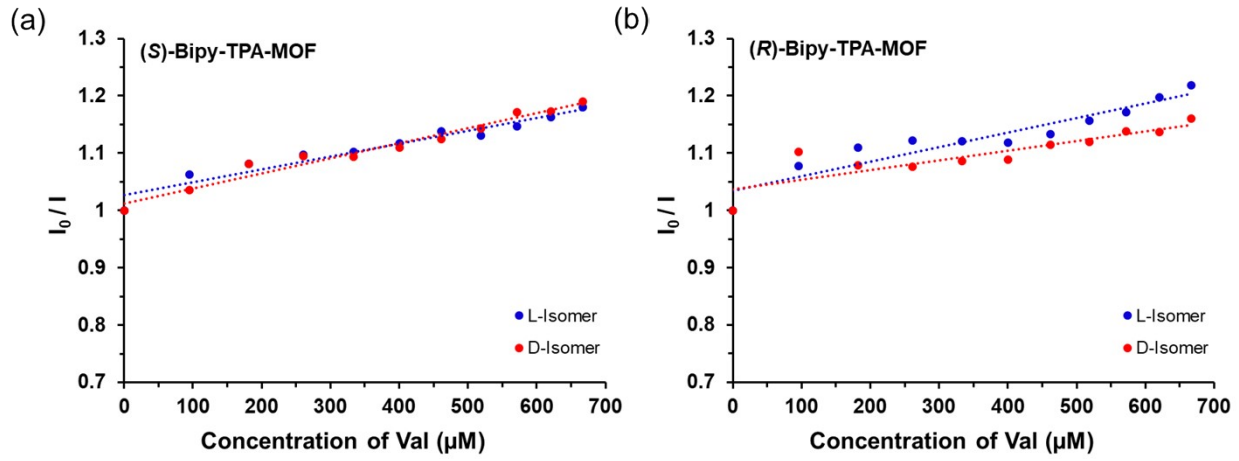

Figure S34. Stern-Volmer plots of (a) **(*S*)-1** and (b) **(*R*)-1** with the enantiomers of valine (**Val**)

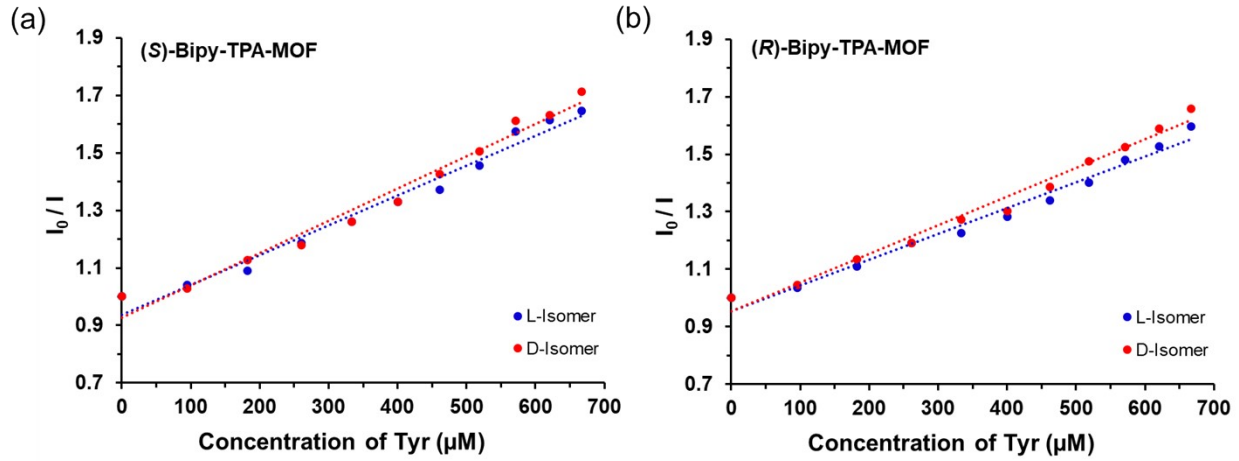

Figure S35. Stern-Volmer plots of (a) **(*S*)-1** and (b) **(*R*)-1** with the enantiomers of tyrosine (**Tyr**).

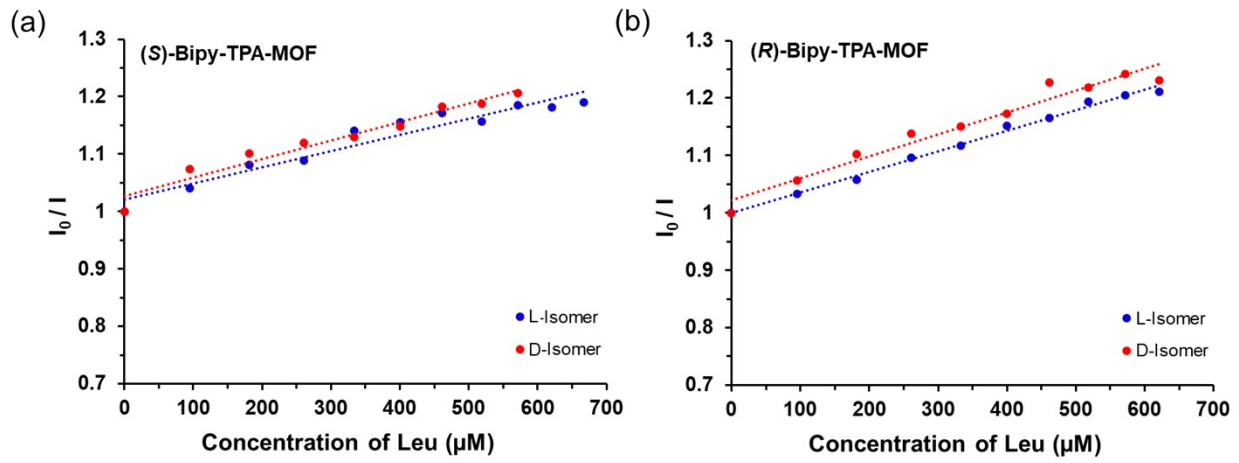

Figure S36. Stern-Volmer plots of (a) **(S)-1** and (b) **(R)-1** with the enantiomers of leucine (**Leu**).

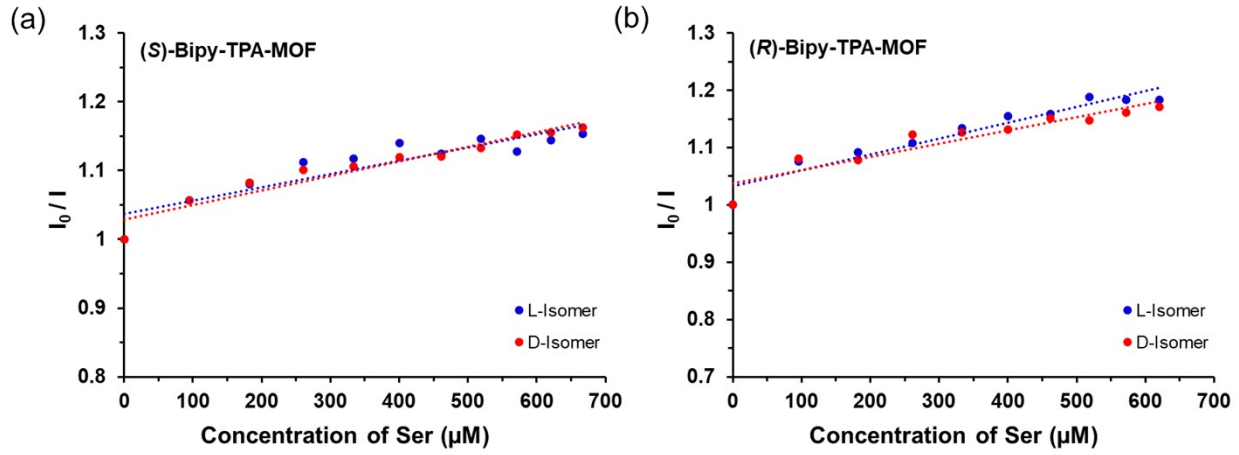

Figure S37. Stern-Volmer plots of (a) **(S)-1** and (b) **(R)-1** with the enantiomers of serine (**Ser**).

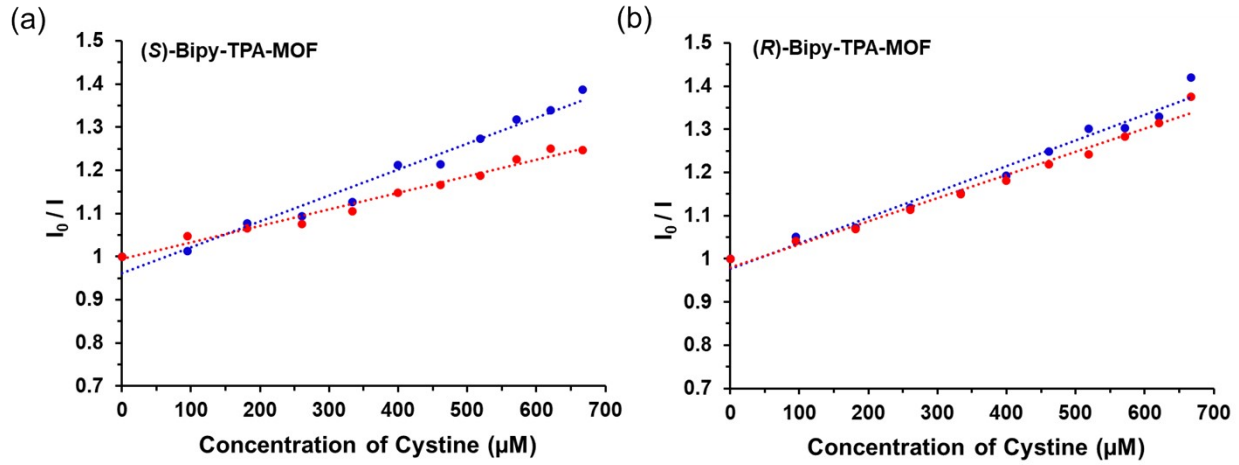

Figure S38. Stern-Volmer plots of (a) **(S)-1** and (b) **(R)-1** with the enantiomers of cystine.

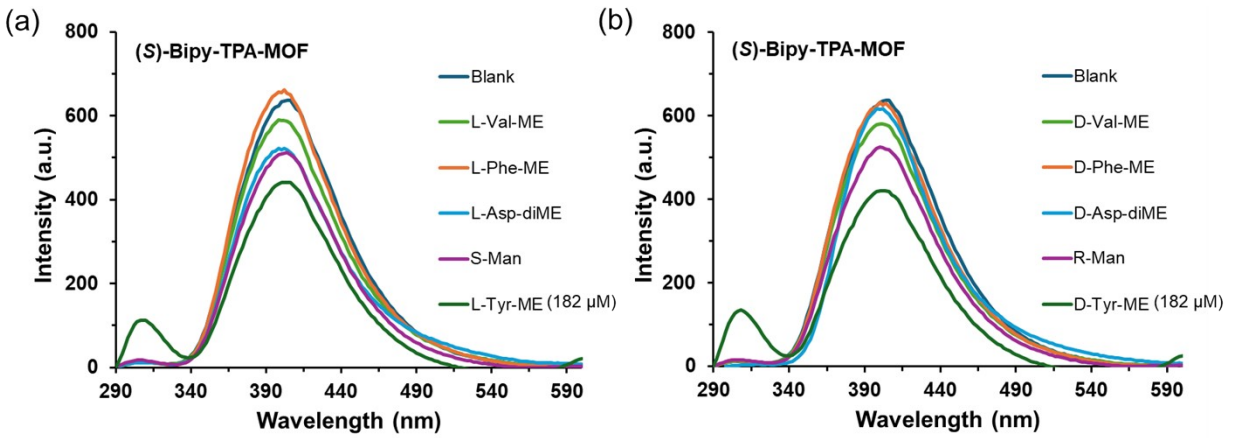

Figure S39. The fluorescence spectra of **(*S*)-1** (0.2 g·L-1) with various (a) (*L*)-amino acid esters hydrochloride and **(*S*)-Man**, (b) (*D*)-amino acid esters hydrochloride and **(*R*)-Man** (520 μM) with an excitation wavelength (λ_{ex}) of 270 nm. Tyrosine methyl ester hydrochloride was an exception, used at a concentration of 182 μM.

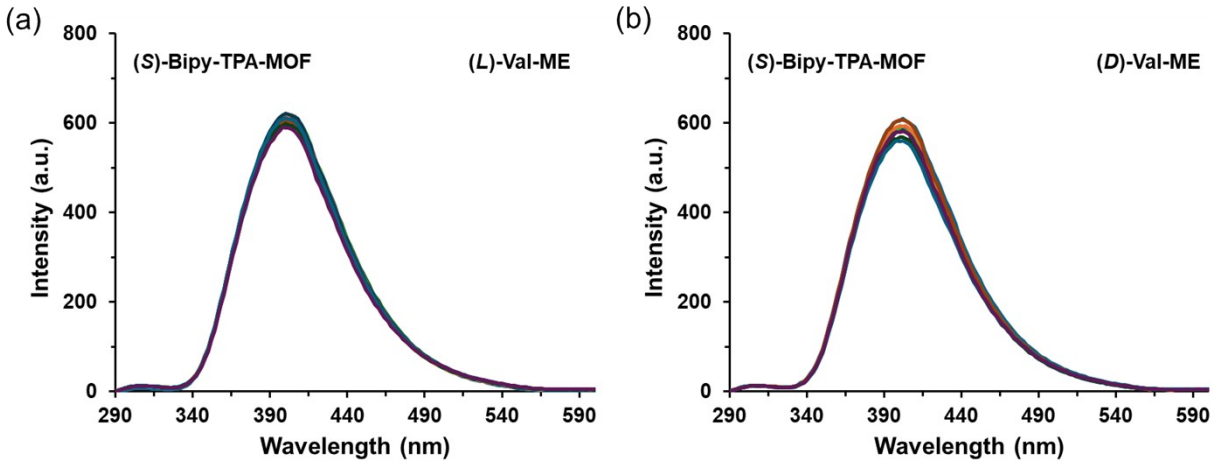

Figure S40. Fluorescence titration spectra of **(*S*)-1** with (a) **(*L*)-Val-ME** and (b) **(*D*)-Val-ME,** ranging from 0 μM to 667 μM of analyte.

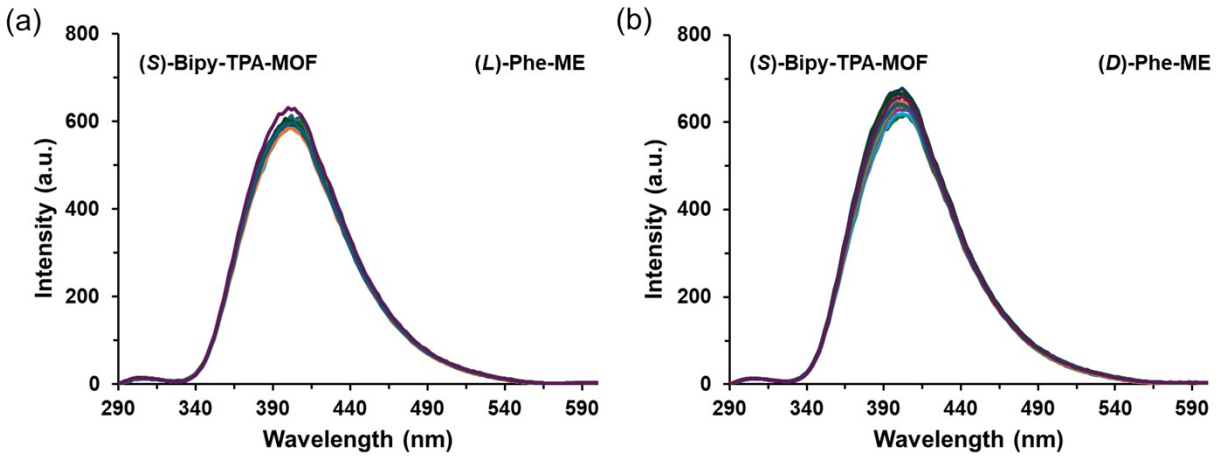

Figure S41. Fluorescence titration spectra of **(*S*)-1** with (a) **(*L*)-Phe-ME** and (b) **(*D*)-Phe-ME,** ranging from 0 μM to 667 μM of analyte.

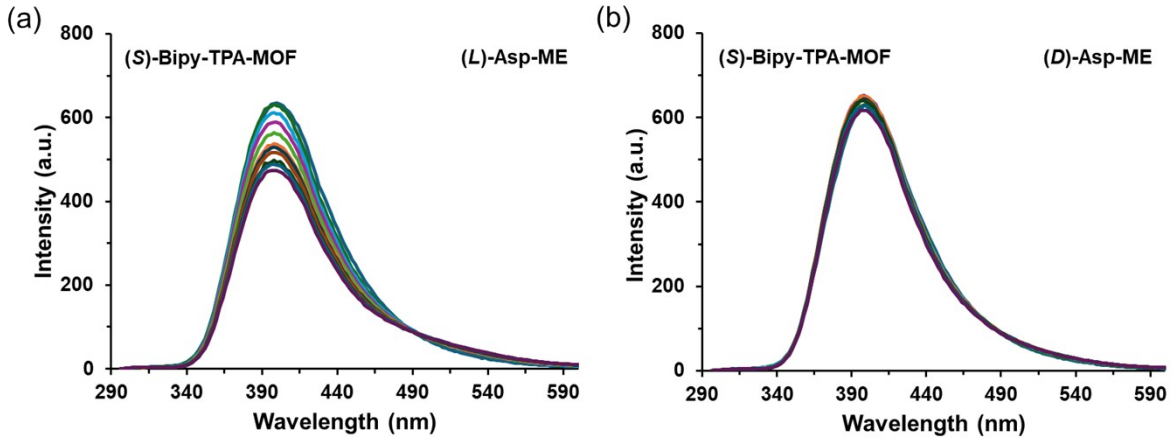

Figure S42. Fluorescence titration spectra of **(*S*)-1** with (a) **(*L*)-Asp-ME** and (b) **(*D*)-Asp-ME,** ranging from 0 μM to 667 μM of analyte.

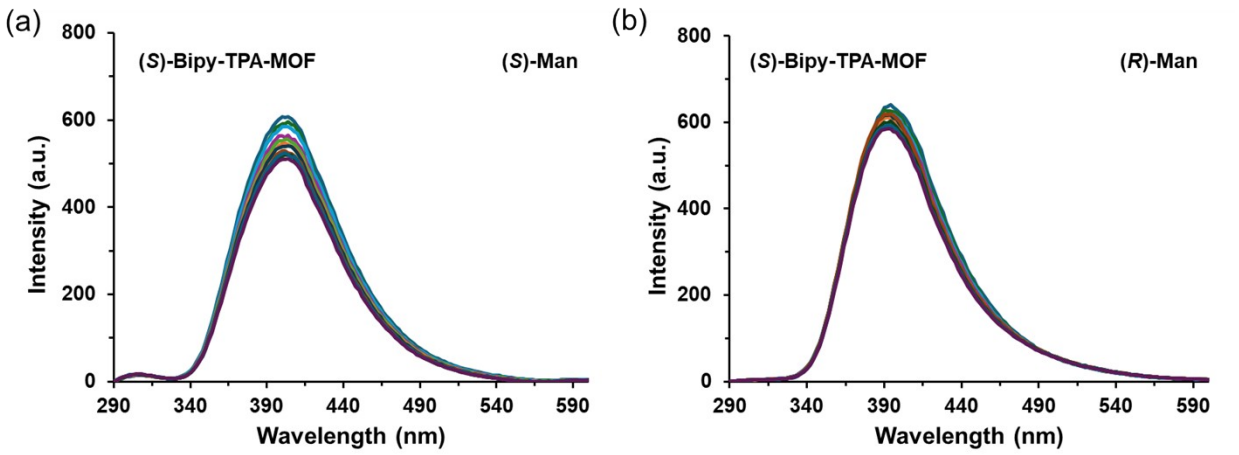

Figure S43. Fluorescence titration spectra of **(*S*)-1** with (a) **(*S*)-Man** and (b) **(*R*)-Man,** ranging from 0 μM to 667 μM of analyte.

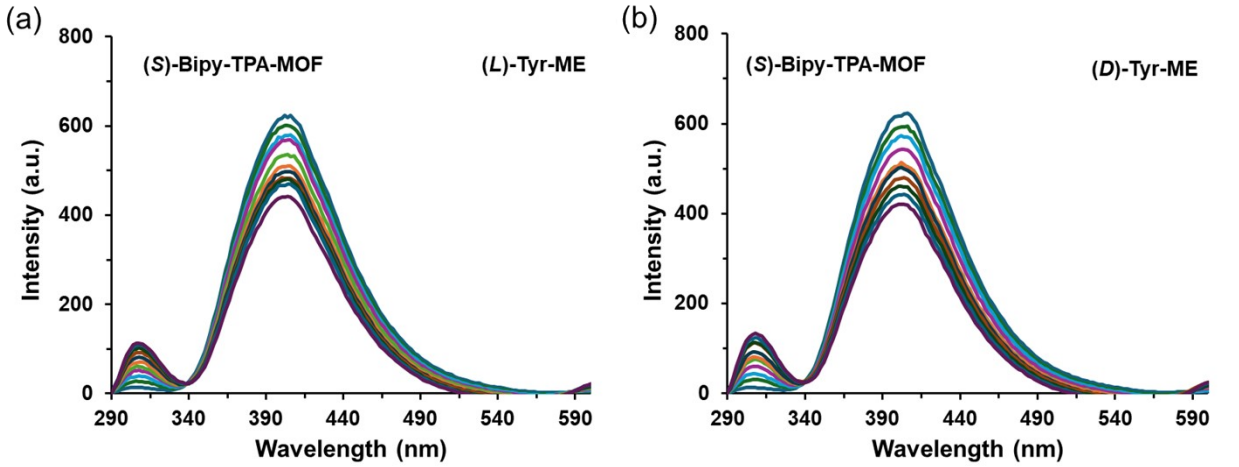

Figure S44. Fluorescence titration spectra of **(*S*)-1** with (a) **(*L*)-Tyr-ME** and (b) **(*D*)-Tyr-ME,** ranging from 0 μM to 182 μM of analyte.

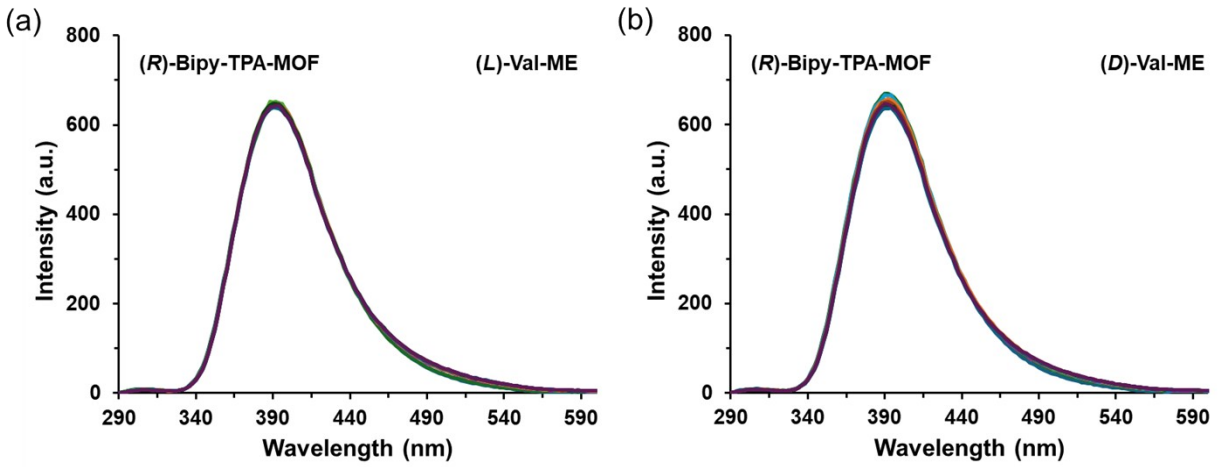

Figure S45. Fluorescence titration spectra of **(*R*)-1** with (a) **(*L*)-Val-ME** and (b) **(*D*)-Val-ME,** ranging from 0 μM to 667 μM of analyte.

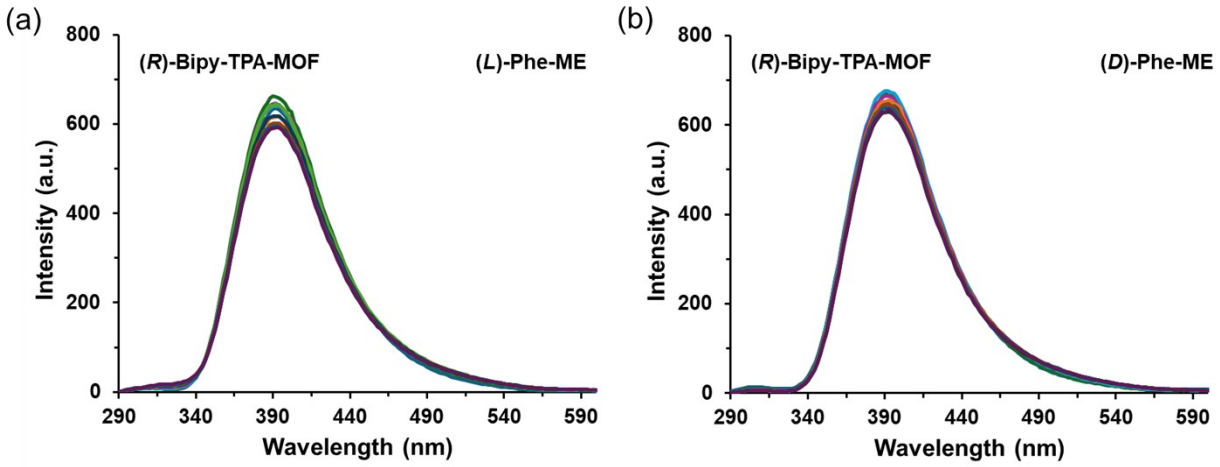

Figure S46. Fluorescence titration spectra of **(*R*)-1** with (a) **(*L*)-Phe-ME** and (b) **(*D*)-Phe-ME,** ranging from 0 μM to 667 μM of analyte.

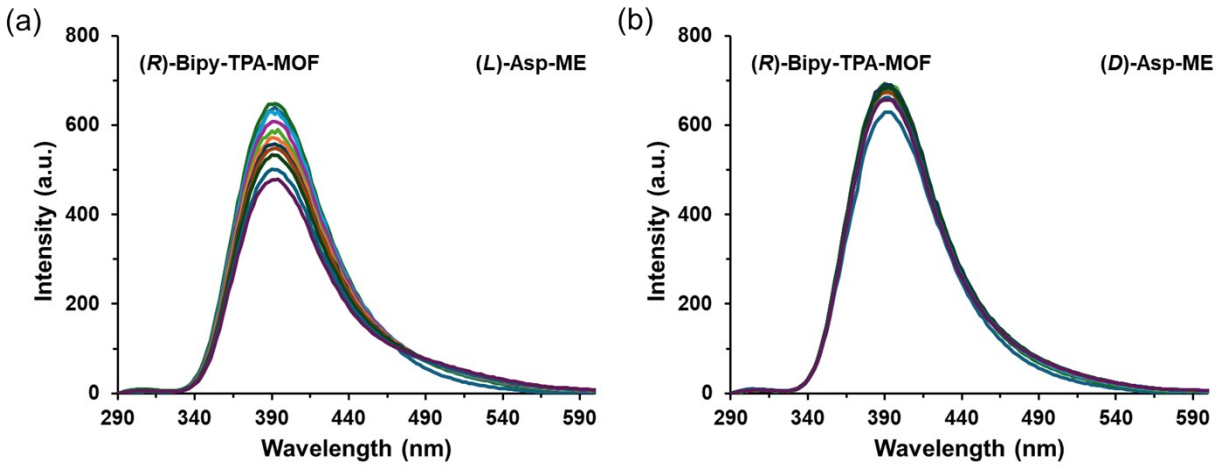

Figure S47. Fluorescence titration spectra of **(*R*)-1** with (a) **(*L*)-Asp-ME** and (b) **(*D*)-Asp-ME,** ranging from 0 μM to 667 μM of analyte.

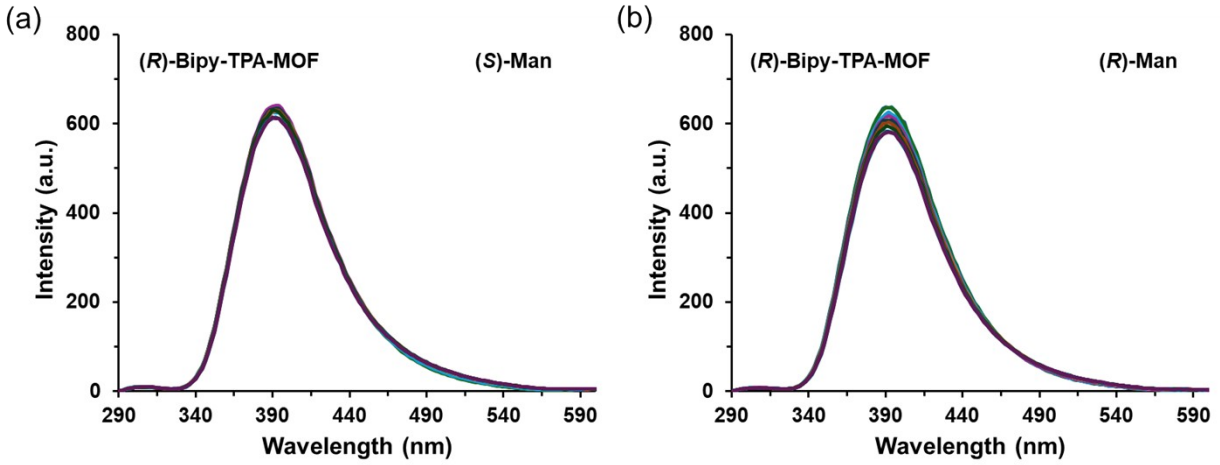

Figure S48. Fluorescence titration spectra of **(*R*)-1** with (a) **(*S*)-Man** and (b) **(*R*)-Man,** ranging from 0 μM to 667 μM of analyte.

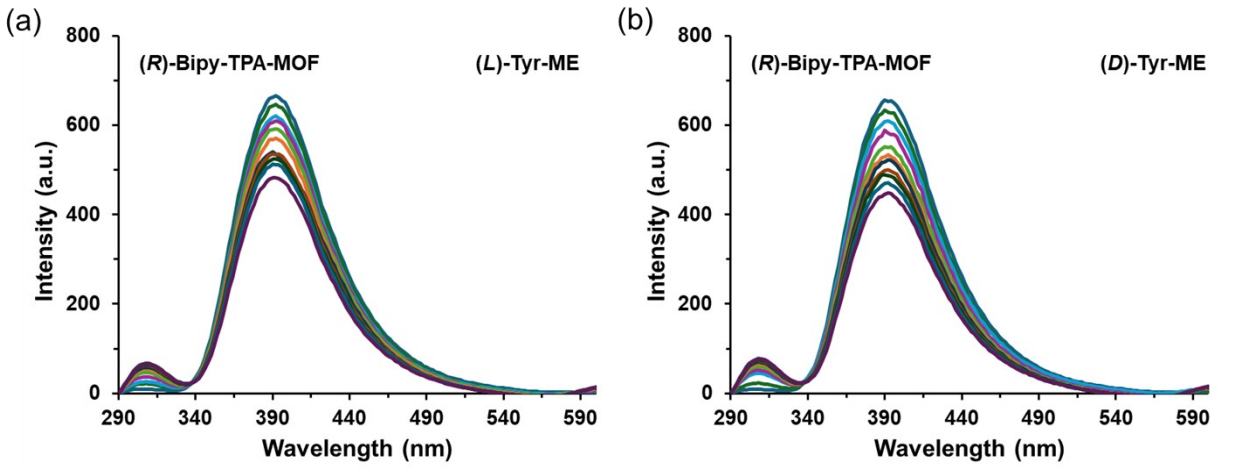

Figure S49. Fluorescence titration spectra of **(*R*)-1** with (a) **(*L*)-Tyr-ME** and (b) **(*D*)-Tyr-ME,** ranging from 0 μM to 182 μM of analyte.

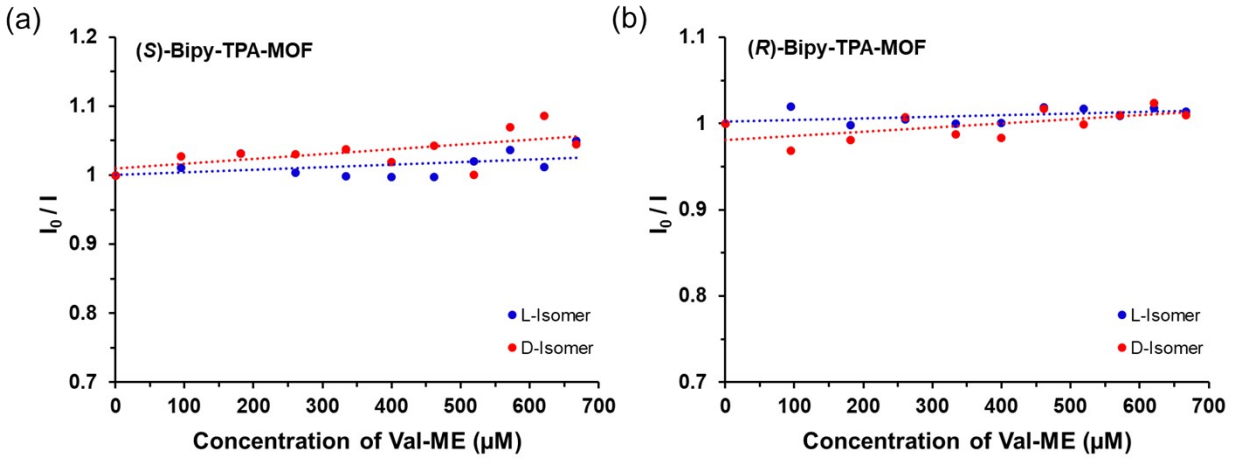

Figure S50. Stern-Volmer plots of (a) **(*S*)-1** and (b) **(*R*)-1** with the enantiomers of **Val-ME.**

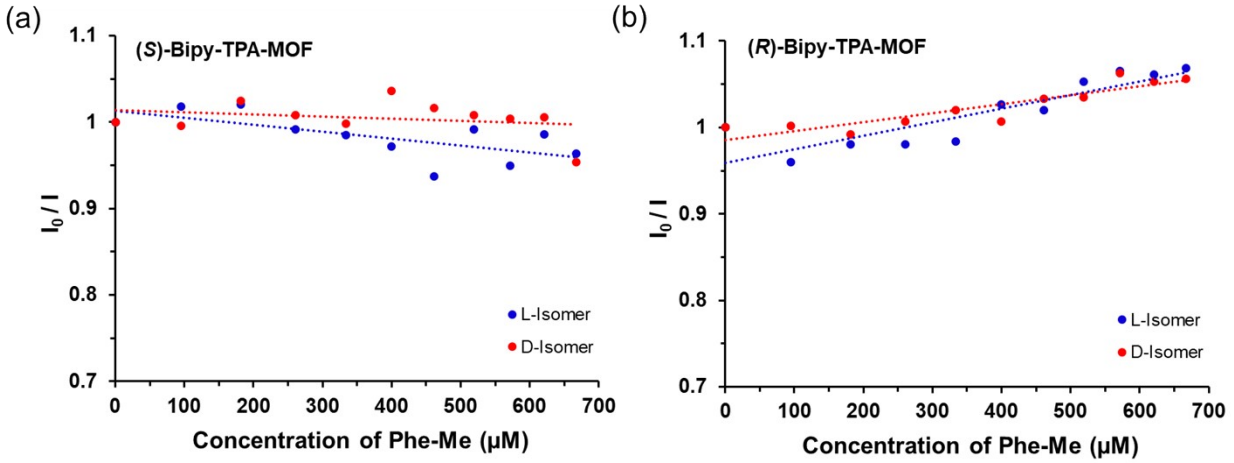

Figure S51. Stern-Volmer plots of (a) **(*S*)-1** and (b) **(*R*)-1** with the enantiomers of **Phe-ME.**

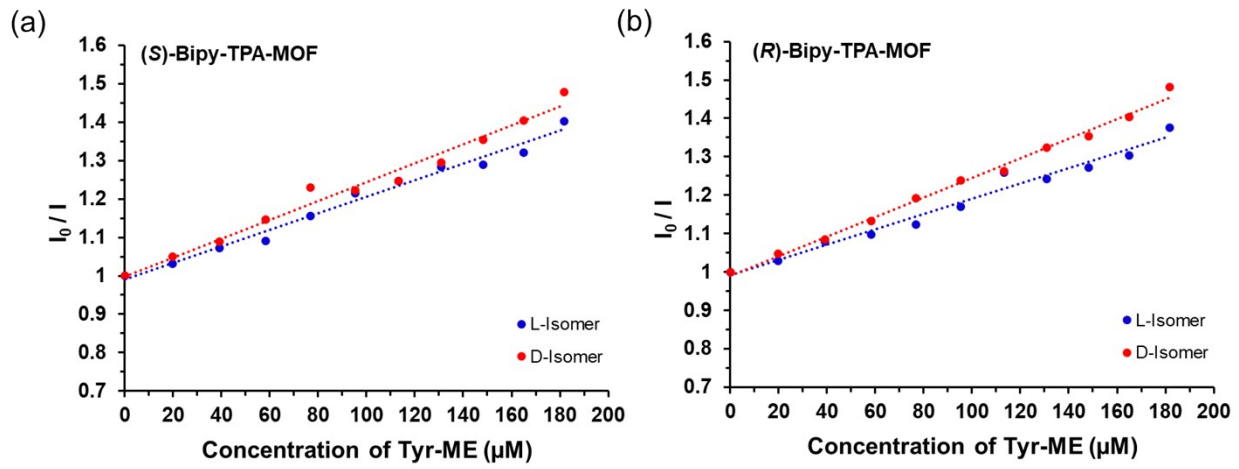

Figure S52. Stern-Volmer plots of (a) **(*S*)-1** and (b) **(*R*)-1** with the enantiomers of **Tyr-ME.**

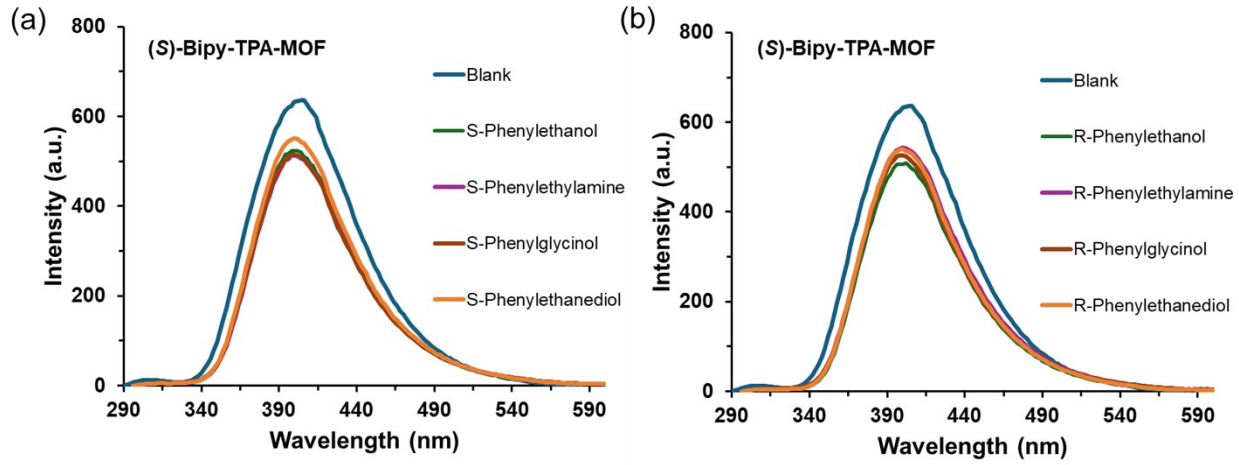

Figure S53. The fluorescence spectra of **(*S*)-1** (0.2 g·L^{-1}) with various (a) (*S*)-amino and hydroxy substituted ethylbenzene, (b) (*R*)-amino and hydroxy substituted ethylbenzene (667 μM) with an excitation wavelength (λ_{ex}) of 270 nm.

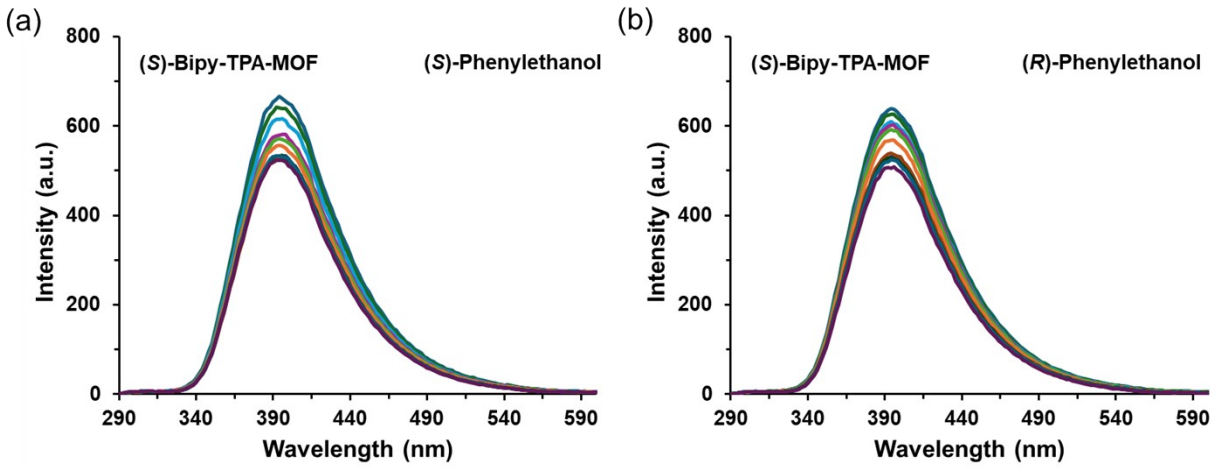

Figure S54. Fluorescence titration spectra of **(*S*)-1** with (a) (*S*)-Phenylethanol and (b) (*R*)-Phenylethanol**,** ranging from 0 μM to 667 μM of analyte.

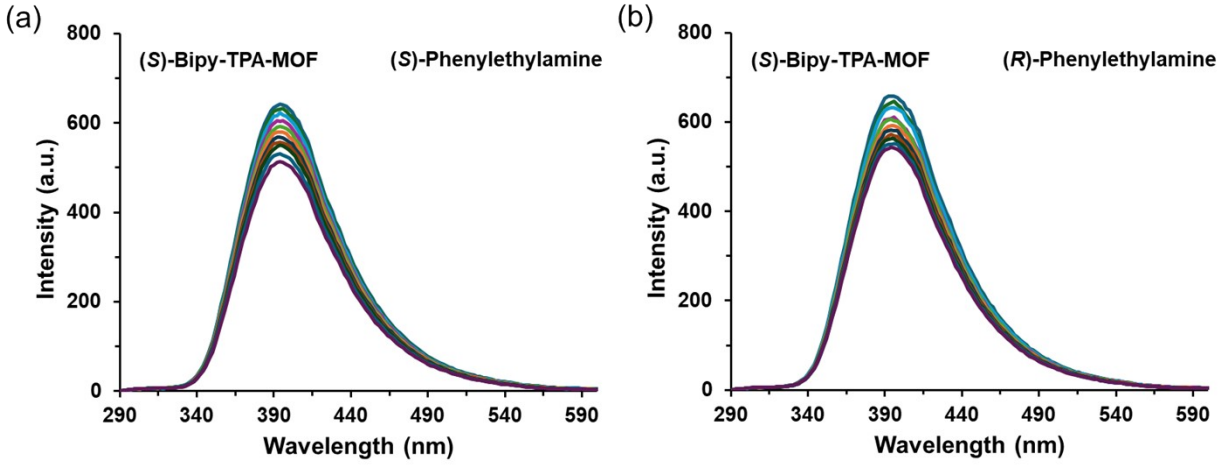

Figure S55. Fluorescence titration spectra of **(*S*)-1** with (a) (*S*)-Phenylethylamine and (b) (*R*)-Phenylethylamine**,** ranging from 0 μM to 667 μM of analyte.

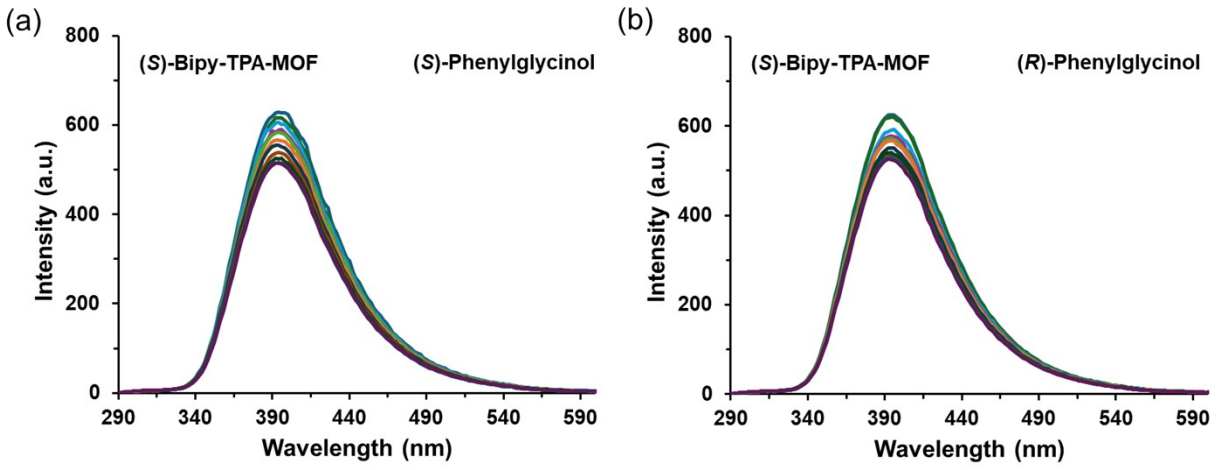

Figure S56. Fluorescence titration spectra of **(*S*)-1** with (a) (*S*)-Phenylglycinol and (b) (*R*)-Phenylglycinol**,** ranging from 0 μM to 667 μM of analyte.

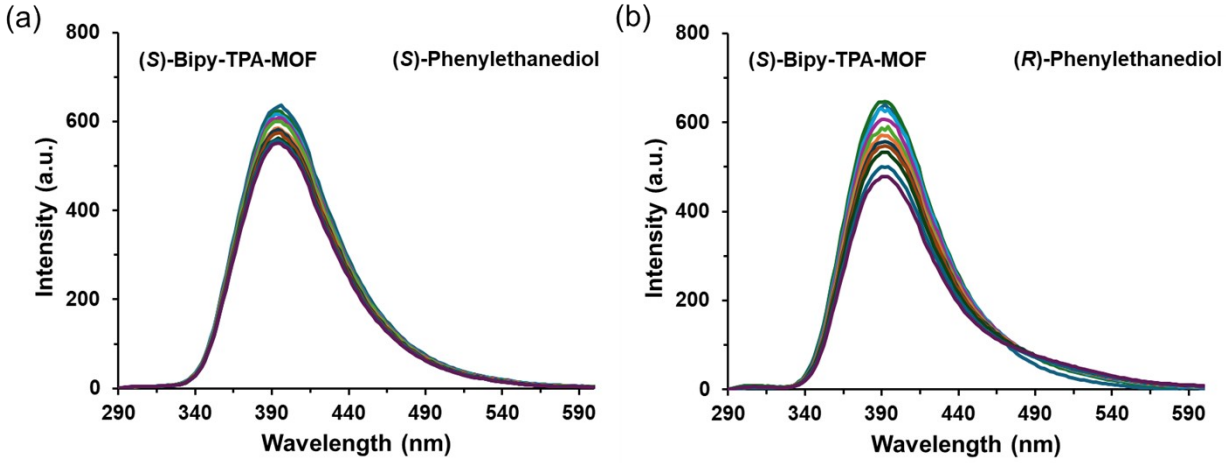

Figure S57. Fluorescence titration spectra of **(*S*)-1** with (a) (*S*)-Phenylethanediol and (b) (*R*)-Phenylethanediol**,** ranging from 0 μM to 667 μM of analyte.

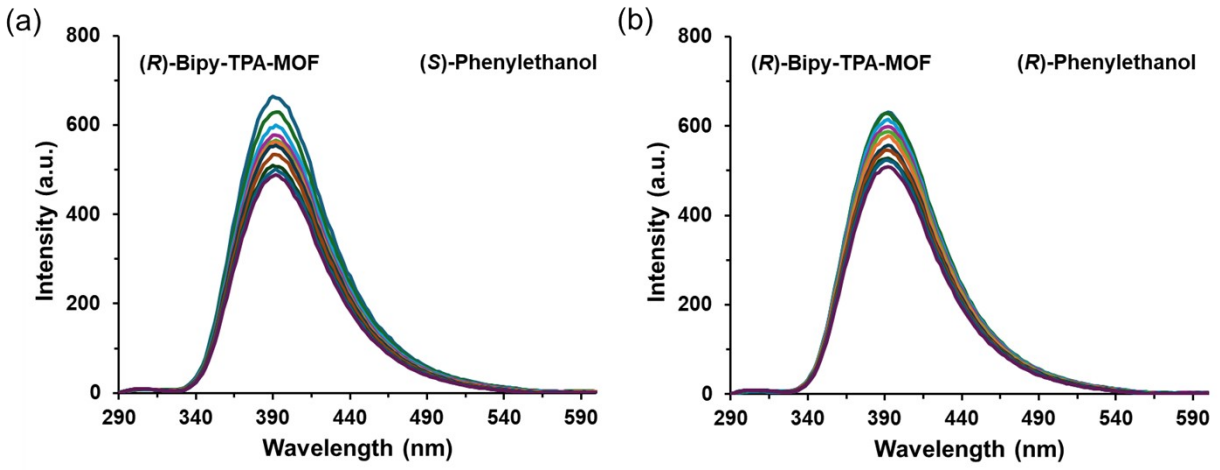

Figure S58. Fluorescence titration spectra of **(*R*)-1** with (a) (*S*)-Phenylethanol and (b) (*R*)-Phenylethanol**,** ranging from 0 μM to 667 μM of analyte.

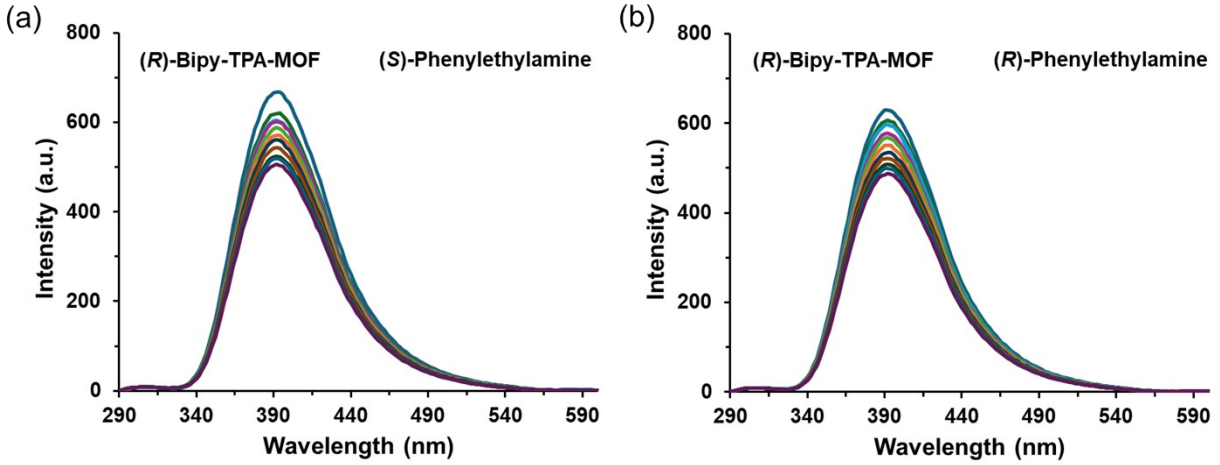

Figure S59. Fluorescence titration spectra of **(*R*)-1** with (a) (*S*)-Phenylethylamine and (b) (*R*)-Phenylethylamine**,** ranging from 0 μM to 667 μM of analyte.

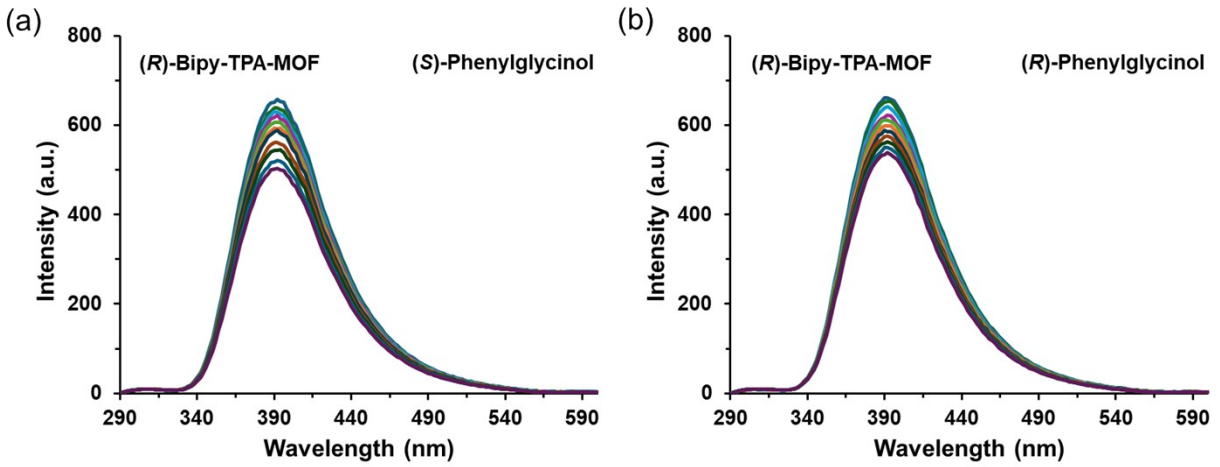

Figure S60. Fluorescence titration spectra of **(*R*)-1** with (a) (*S*)-Phenylglycinol and (b) (*R*)-Phenylglycinol**,** ranging from 0 μM to 667 μM of analyte.

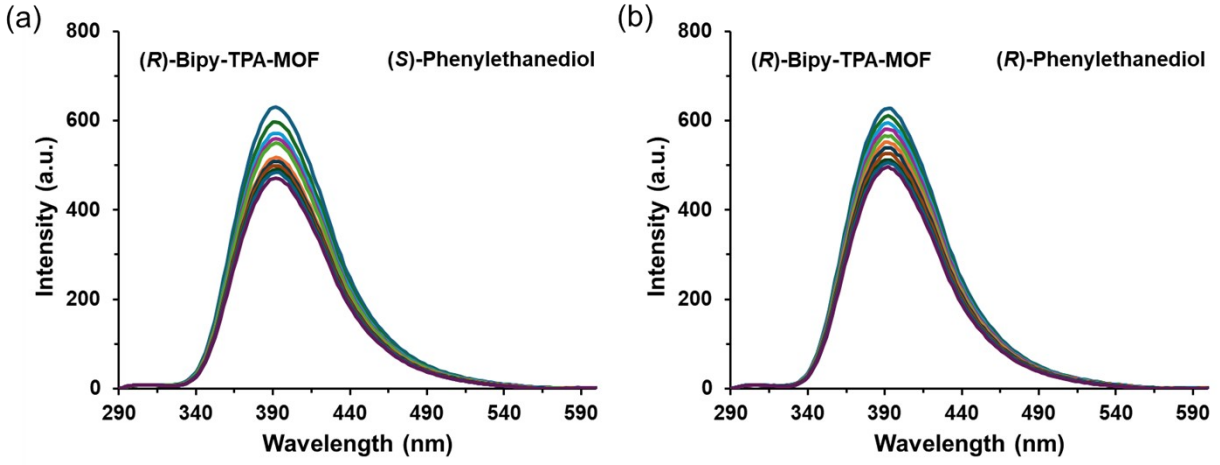

Figure S61. Fluorescence titration spectra of **(*R*)-1** with (a) (*S*)-Phenylethanediol and (b) (*R*)-Phenylethanediol**,** ranging from 0 μM to 667 μM of analyte.

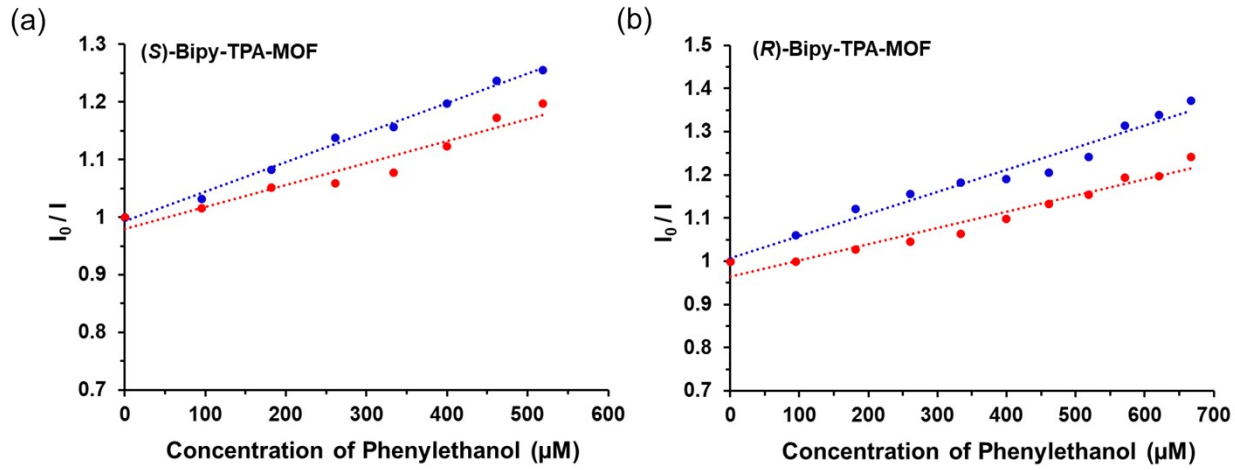

Figure S62. Stern-Volmer plots of (a) **(*S*)-1** and (b) **(*R*)-1** with the enantiomers of phenylethanol.

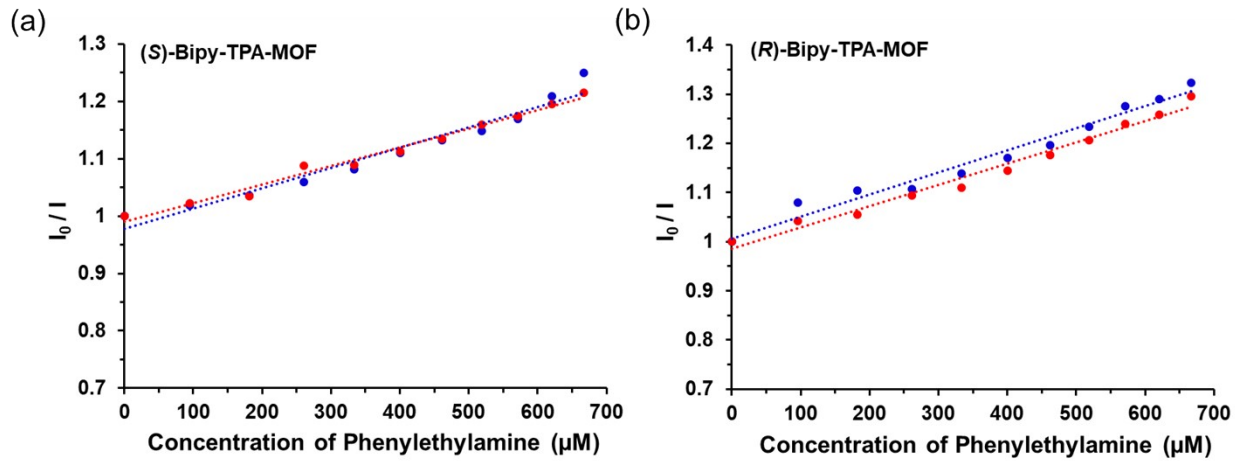

Figure S63. Stern-Volmer plots of (a) **(*S*)-1** and (b) **(*R*)-1** with the enantiomers of phenylethylamine.

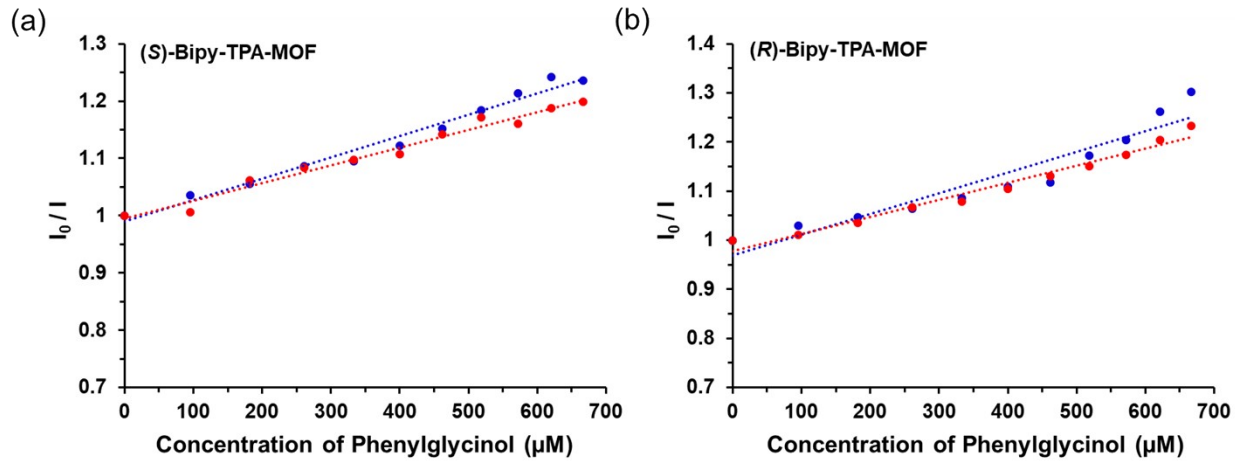

Figure S64. Stern-Volmer plots of (a) **(*S*)-1** and (b) **(*R*)-1** with the enantiomers of phenylglycinol.

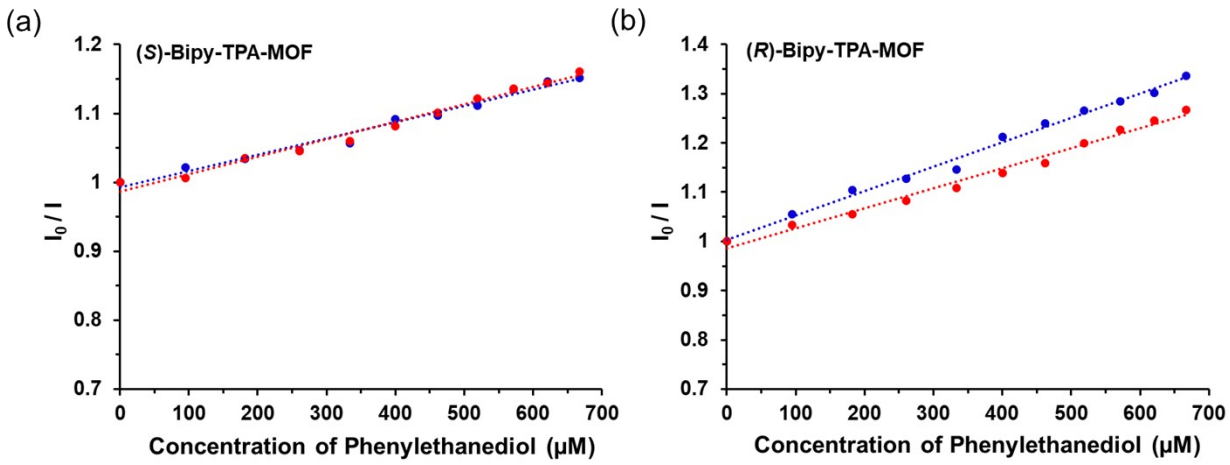

Figure S65. Stern-Volmer plots of (a) **(*S*)-1** and (b) **(*R*)-1** with the enantiomers of phenylethanediol.

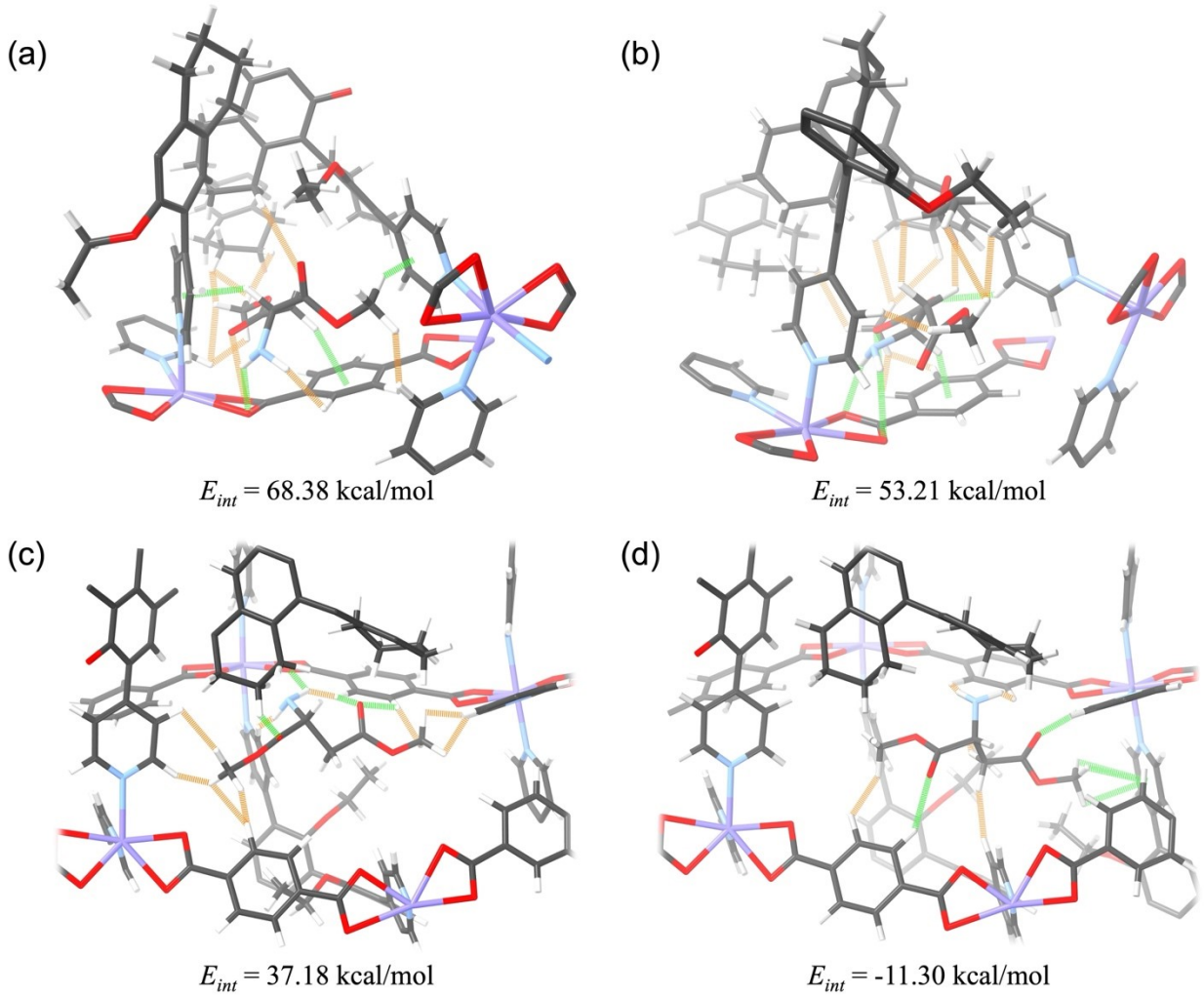

Figure S66: Optimised geometries and interaction energies (E_{int}) of **(*S*)-1** interacting with **(*L*)-**aspartic acid dimethyl ester (**(*L*)-Asp-diME**). Panels (a) and (b) depicts the **(*L*)-Asp-diME** within the smaller channel, while (c) and (d) show the **(*L*)-Asp-diME** positioned in the larger channel. The carbon, oxygen, nitrogen, and hydrogen atoms are represented in black, red, blue and white, respectively. Green dashed lines represent attractive interactions while orange dashed lines represent repulsive interaction.

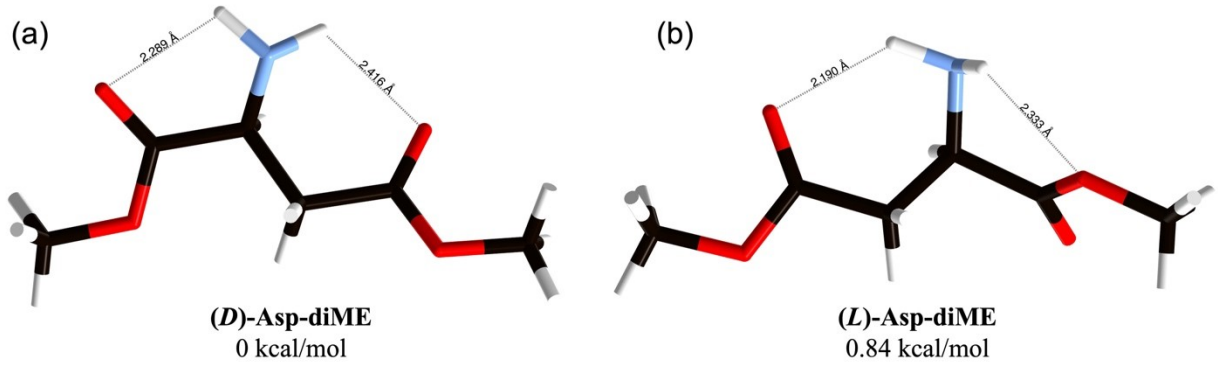

Figure S67: Optimised geometries and relative energies of (a) **(*D*)**-aspartic acid dimethyl ester **(Asp-diME)**. (b) **(*L*)-Asp-diME**. The carbon, oxygen, nitrogen, and hydrogen atoms are represented in black, red, blue and white, respectively.

References

(1) Turlington, M.; DeBerardinis, A. M.; Pu, L. Highly Enantioselective Catalytic Alkyl Propiolate Addition to Aliphatic Aldehydes. *Org. Lett.* **2009**, *11* (11), 2441-2444. DOI: 10.1021/ol900667g.